AN ABSTRACT OF THE THESIS OF

Shuh-Ren Lin for the degree of Doctor of Philosophy in Mechanical Engineering presented on April 18, 1985

Title: Wind Turbulence Input Model for Horizontal Axis Wind Turbines

Abstract approved: Redacted for privacy

Dr. William E. Holley

In order to estimate wind turbine response characteristics in the presence of atmospheric turbulence, the important atmospheric sources for the force excitations felt by the wind turbine system must be identified and characterized. The goal of this research is to develop the wind turbulence input model for horizontal axis wind turbines.

The wind turbulence inputs are determined in three basic modeling steps. First, the turbulent velocity field is assumed to be stationary, locally homogeneous, isotropic, and satisfying Taylor's frozen field hypothesis. The Von Karman model is used to characterize the correlation between velocity components at different spatial positions and at different times. The procedure for finding the aerodynamic forces and moments which are caused by the turbulence, is complicated by the distribution of the turbulent velocity across each of the wind turbine blades. In the second step, the spatial variation of the turbulence is approximated by a few terms in a

series expansion. Here, uniform terms across the rotor disk, gradient terms which vary linearly across the disk, and terms which vary quadratically across the disk are retained. All of these terms are time dependent. In the third step, the correlation of these turbulent velocity terms can be closely approximated by low order linear systems forced by white noise.

The resulting turbulence input model is then validated using the forward square root information filter and the backward square root information smoother. The residuals between the model outputs and actual field tests are calculated and presented in terms of power spectral density functions.

Wind Turbulence Input Model for Horizontal Axis Wind Turbines

by

Shuh-Ren Lin

A THESIS

submitted to

Oregon State University

in partial fulfillment of
the requirements for the
degree of

Doctor of Philosophy

Completed April 18, 1985

Commencement June 1985

APPROVED:

Redacted for privacy

Professor of Mechanical Engineering in charge of major

Redacted for privacy

Head of Department of Mechanical Engineering

Redacted for privacy

Dean of Graduate School

Date thesis is presented April 18, 1985

Typed by Opal Grossnicklaus for Shuh-Ren Lin

ACKNOWLEDGEMENTS

I wish to acknowledge the individuals and faculty of Mechanical Engineering at Oregon State University who helped make this dissertation paper possible.

Dr. William E. Holley, my major professor, has been the major impetus for this accomplishment. I appreciate his help and guidance.

I wish to thank my parents for their support and my wife, Florence, for her encouragement.

I would also like to thank my committee members: Dr. Robert Wilson, Dr. F. Tom Lindstrom, Dr. Timothy C. Kennedy, and Dr. Alan Robinson for taking their time to serve on my committee.

Finally, I would like to thank the Oregon State University Computer Center for providing computer time through unsponsored research funds.

LIST OF SYMBOLS

a	Constant used in the Von Karman correlation function
A	Rotor disk area
$A(k)$	pxp upper triangular matrix in information filter time update
$A^{(i)}(k)$	Scalar, see Eq. (4.54)
b	Constant used in the Von Karman correlation function
$b(k)$	n vector equal to $W(k)x(k)$
$B^{(i)}(k)$	lxn matrix, see Eq. (4.54)
C	mxn measurement matrix
$C(k)$	C at stage k
$c^{(i)}(k)$	Scalar, see Eq. (4.54)
$d(k)$	$Y(k)\hat{x}(k)$
e_n	The approximation error including only nth order terms of turbulence velocity
$e(k)$	m vector residual
$E(k)$	$\phi^{-T}Y(k)\phi^{-1}$
f_i	Weight function
$F(k)$	$W(k+)\phi^{-1}\Gamma$
$G(k)$	$[F^T(k)F(k)+Q]^{T/2}$
$H(\cdot)$	Frequency response function
i	$\sqrt{-1}$
I	Identity matrix

I_n	mxn identity matrix
J	Scalar cost function
K_i	Constants defined in text
K	nxm covariance filter gain matrix
L	integral scale of the turbulence
L	nxp information filter gain matrix (Sec. IV.3.2)
m	Dimension of y
n	Dimension of x
N	Number of stages in the smoothing problem
p	Dimension of u
P(k)	nxn error covariance of x(k)
Q(k)	pxp covariance of u(k)
R	Rotor disk radius
R(k)	mxn covariance of v(k)
R(•)	Correlation
R_{ij}	Elements of correlation tensor for the wind velocity at two points
R_*	R/L
S_w	Power spectral density of white noise
t	Time
T(•)	Transfer function
u(k)	p vector process noise
U,U(k)	$UU^T = Q$
v_i	The turbulence velocity
v(k)	m vector measurement
V,V(k)	$VV^T = R$
V_i	Uniform turbulent term

$V_{i,j}$ Gradient turbulent term

$V_{i,jk}$ Quadratic turbulent term

V_w Mean wind speed

w Nondimensional white noise

x Lateral coordinate

y Longitudinal coordinate

Y(k) nxn information matrix, $Y = P^{-1}$

z Vertical coordinate

Greek symbols:

γ Empirical constant

$\vec{\xi}$ Separation vector between the two spatial points

ξ_i ith component of the vector $\vec{\xi}$

ξ Magnitude of $\vec{\xi} = \sqrt{\xi_1^2 + \xi_2^2 + \xi_3^2}$

η $\sqrt{\xi^2 + V_w^2 \tau^2}$

μ $\sqrt{(\frac{\omega\xi}{V_w})^2 + (\frac{\xi}{aL})^2}$

τ Time interval

σ^2 Turbulent velocity component variance

δ_{ij} Kronecker delta (1 for i = j and 0 for i = j)

γ_{xz} Swirl about mean wind axis (in-plane turbulent input)

$\bar{\gamma}_{xz}$ In-plane shear strain rate (turbulence input)

ϵ_{xz} In-plane shear strain rate (turbulence input)

$\bar{\epsilon}_{xz}$ In-plane dilating (turbulence input)

Γ nxp noise influence matrix

Δ Sampling period

ϕ Transition matrix

Φ_{ij}	Normalized complex cross-spectrum
ω	Radian frequency
π	3.1415

Mathematical symbols:

$\|\|( )\|\|$	Euclidian vector norm of ( )
$\triangleq$	Defined equal to
$\approx$	Approximately equal to

Subscripts

k	The kth stage or kth component
k/N	At stage k given measurements through N
+	After incorporating the measurement
k+	After incorporating y(k)

Superscripts

-1	Matrix inverse
T	Matrix transpose
^	Best estimate
k	On the kth iteration

Special functions and operators:

exp(•)	Exponential function
E[•]	Expectation operator
$K_{1/3}$	Modified Bessel function of order 1/3
$\Gamma(\bullet)$	Gamma function
Σ	Summation operator

TABLE OF CONTENTS

LIST OF FIGURES

LIST OF TABLES

WIND TURBULENCE INPUT MODEL FOR HORIZONTAL AXIS WIND TURBINES

I. INTRODUCTION

The total velocity field for the atmosphere is variable in both space and time, and is composed of a relatively steady component and a fluctuating component. By the steady component, we usually mean a temporal average over some period such as several minutes. These mean wind speeds can be predicted for several days or estimated from climatological data. Because of the drag due to roughness at the ground, the mean wind speed usually increases with increasing height.

The fluctuating part is generally called turbulence. Some basic features of turbulence are not yet explained theoretically, because turbulence is a strongly nonlinear phenomenon and a stochastic process (1, 2). We cannot predict the detailed evolution of a turbulent flow, but we can predict some of its statistical properties.

From the early operation of the Mod-0 experimental turbine at the NASA Lewis Research Center, it was identified that atmospheric turbulence is one of the major sources for the dynamic loads for wind turbine operation. Thresher et al. (3) show that turbulence excitations are at least as important as wind shear effects in computing the dynamic response of wind turbines. Due to the

random nature of the atmospheric turbulence, it is a difficult problem to determine the fluctuations in the aerodynamic forces acting on a wind turbine rotor blade. This work focuses on using statistical approaches based on random vibration theory and spectral analysis to develop the turbulent wind input model for horizontal axis wind turbines.

Model assumptions and approximations which will be used for the modeling of atmospheric turbulence are presented in Chapter II. Using an approximation concept, the spatial variation of the turbulence is presented with a few terms of a series expansion. This local approximation of the turbulence field is developed in some detail in Chapter III. In addition, this chapter covers the use of filtered noise as a modeling approximation for the turbulence inputs and provides the necessary data for turbulence inputs for a wide range of wind turbine sizes.

Realistic evaluation of the modeling error, however, can only be accomplished by comparison with experimental data. In Chapter IV, the square root fixed interval smoothing methods are applied to the turbulence input model. The residuals between the model outputs and observations are calculated and discussed.

II. MODELING OF ATMOSPHERIC TURBULENCE

II.1 Introduction

Since the turbulence is a random process that cannot be described by explicit functions of position and time, only a statistical approach can be taken. For a complete statistical description, all of the joint probability distributions of each turbulent velocity fluctuation at all points in the spatial and time domain of consideration are required. Clearly, such a description will not be tractable without simplifying assumptions. One appealing simplification is to approximate the distribution as normal or Gaussian. With this assumption, the needed statistics of the turbulence are completely described by the correlations among the velocity components at different points in space and at different time instants. This correlation in general is expressed as the second rank tensor

$$R_{ij}(\vec{\xi},\vec{x},\tau,t) \triangleq E[v_i(\vec{x}+\vec{\xi},\ t+\tau)v_j(\vec{x},t)] \tag{2.1}$$

where $v_i(\vec{x},t)$ = ith velocity component at position, $\vec{x}$, and time, t.

$\vec{\xi}$ = separation vector between the two spatial points

τ = time interval

$E[\cdot]$ = expected value operator.

From the correlation function and its Fourier transform, the spectrum function, it is assumed that all the pertinent results can

be derived. The principal objective of this research into atmospheric turbulence is to ascertain the appropriate mathematical forms for the correlation function and spectrum function.

II.2 Simplifying Assumptions

Although there is some evidence that atmospheric turbulence is not necessarily normal or Gaussian (4), many researchers have concluded that for practical purposes it may be approximated as Gaussian in many situations. We therefore assume that the random functions we have to deal with follow normal distributions.

Upon examination of the definition of the correlation function (Eq. 2.1), it is evident that a tremendous amount of information is still required. For three dimensional turbulence, the correlation function represents six independent functions of eight real variables (the space-time coordinates of the two points). In order to quantify these relationships considerable further simplification is required.

One simplification usually employed (5, 6) when modeling atmospheric turbulence, is the Taylor frozen field hypothesis (7). In 1938 G. I. Taylor postulated that if the mean wind speed were high enough, the turbulence would not have time to change as it was being convected past a point. Thus, the correlations are given simply by the spatial separation between points in a reference frame moving with the mean wind, and

$$R_{ij}(\vec{\xi},\vec{x},\tau,t) = R_{ij}(\vec{\xi}-\vec{v}_w\tau,\ \vec{x},0,t) \qquad (2.2)$$

where $\vec{v}_w$ is the mean wind velocity. For stationary turbulence, when

the statistics are time invariant, the explicit dependence on time is dropped.

II.3 Locally Homogeneous and Isotropic Correlation Model

A turbulent flow is homogeneous if its statistics are invariant under translation of the spatial coordinate frame. If the statistics are invariant to changes in directions of the coordinates as well, then it is isotropic. The assumptions of homogeneity and isotropy which are often used in analysis involving aircraft flying through turbulence (8, 9) are more questionable when applied to turbulence observed in the atmospheric boundary layer.

The characteristic turbulent eddy size tends to increase with height above the ground (10) indicating inhomogeneity in the vertical direction. Also the variances of the velocity components in the atmospheric boundary layer are not equal and the longitudinal and vertical velocity components are correlated near the ground (11), each of which indicates that isotropy is violated. However, when the spatial separations are small, it is expected that the behavior is approximately homogeneous and isotropic (12). This local isotropy leads to the so called inertial subrange (13) in which no production and no dissipation of energy takes place. When only this inertial transfer of energy to smaller and smaller eddies is occurring, Kolmogorov (14) suggested that the autocorrelation function for velocity components should be of the form

$$R(\xi) = \sigma^2(1-c\xi^{2/3}) \qquad (2.3)$$

where $R(\xi)$ is the correlation between velocity components in the same direction at points separated by the distance, ξ. The component variance is σ^2 and c is constant. This form leads to the -5/3 power law observed in the inertial subrange for the turbulent velocity component power spectral densities (15, 16). The arguments led Von Karman (17) to postulate the following form for the longitudinal component power spectral density function

$$\frac{\omega S(\omega)}{\sigma^2} = \frac{2(\frac{\omega L}{V_w})}{[1+(a\frac{\omega L}{V_w})^2]^{5/6}} \tag{2.4}$$

where ω = radian frequency

L = integral scale parameter $\left(\triangleq \int_0^\infty \frac{1}{\sigma^2} R(\xi)d\xi\right)$

$$a = \frac{\Gamma(\frac{1}{3})}{\sqrt{\pi}\,\Gamma(\frac{5}{6})} \quad (\approx 1.339)$$

$\Gamma(\cdot)$ = gamma function.

Since the autocorrelation function is the inverse Fourier transform of the spectral density, then $R(\xi)$ can be written as

$$R(\xi) = \frac{1}{2\pi} \int_{-\infty}^{\infty} S(\omega) e^{i(\frac{\omega\xi}{V_w})} d\omega \tag{2.5}$$

and Von Karman's spectrum function results in the autocorrelation function

$$R(\xi) = \sigma^2 b(\frac{\xi}{aL})^{1/3} K_{1/3}(\frac{\xi}{aL}) \tag{2.6}$$

where $b = \frac{2^{\frac{2}{3}}}{\Gamma(1/3)}$ (≈ 0.5925)

$K_{1/3}$ = modified Bessel function of order 1/3.

Since we are interested in the correlations among the different components at different points with an arbitrary three-dimensional separation, it is necessary to consider the full correlation tensor. Batchelor (18) has shown that the condition of isotropy imposes severe restrictions on the form of the correlation tensor. In particular, second rank isotropic tensors depend on two independent scalar functions of Euclidian separation distance, ξ. Thus

$$R_{ij}(\vec{\xi}) = A(\xi)\delta_{ij} + B(\xi)\xi_i\xi_j \tag{2.7}$$

where $\vec{\xi}$ = separation vector in the moving frame

ξ_i = ith component of the vector $\vec{\xi}$

$\xi = |\vec{\xi}| = \sqrt{\xi_1^2 + \xi_2^2 + \xi_3^2}$

$$\delta_{ij} = \begin{cases} 1 & i=j \\ 0 & i\neq j \end{cases} \quad \text{(the Kronecker delta).}$$

Further, the continuity equation for incompressible flow adds an additional relation between the A and B functions resulting in the form

$$R_{ij}(\vec{\xi}) = R(\xi)\,\delta_{ij} + \tfrac{1}{2}\xi R'(\xi)\left(\delta_{ij} - \frac{\xi_i\xi_j}{\xi^2}\right) \tag{2.8}$$

where $R(\xi)$ = the longitudinal correlation function and

$$R'(\xi) = \frac{d}{d\xi}R(\xi).$$

This result is widely used in aircraft studies (19, 20) where the Von Karman function (Eq. 2.6) is used for the longitudinal correlation. In this final form, the correlation between any velocity components at different times and points in space can be computed. It remains to specify the two turbulence parameters σ, L and the mean wind speed V_w.

II.4 Two Point Cross-Spectrum Model

Assuming locally homogeneous and stationary turbulence and Taylor's hypothesis (see Section II.2), a two point velocity cross-spectral density can be defined

$$S_{ij}(\vec{\xi},\omega) = \int_{-\infty}^{\infty} R_{ij}(\vec{\xi}-V_w\tau)e^{-i\omega\tau}\,d\tau \qquad (2.9)$$

where $\vec{\xi}$ is the separation vector between the two points and ω is the radian frequency. The real part is called the cospectrum and the imaginary part the quadrature spectrum. When this function is normalized by the component spectra, we get

$$\Phi_{ij}(\vec{\xi},\omega) = \frac{S_{ij}(\vec{\xi},\omega)}{\sqrt{S_i(\omega)S_j(\omega)}} \qquad (2.10)$$

where $S_i(\omega) = S_{ij}(0,\omega)$ when j=i.

The magnitude of the normalized complex cross-spectrum is the coherence

$$C_{ij}(\vec{\xi}\,\omega) = |\Phi_{ij}(\vec{\xi},\omega)| \qquad (2.11)$$

When the indices i and j are the same and correspond to the longitudinal velocity component and the separation $\vec{\xi}$ is vertical,

Davenport (21) postulates a coherency model of the form

$$C(\xi,\omega) = e^{-\gamma(\frac{\omega\xi}{V_w})} \tag{2.12}$$

where ξ = vertical separation distance

γ = empirical constant ($\approx$1.2).

The Davenport model can be directly compared with a computed form derived from the isotropic Von Karman model of the previous section. In this case,

$$\Phi(\xi,\omega) = \frac{1}{S(\omega)} \int_{-\infty}^{\infty} [R(\eta) + \tfrac{1}{2}\eta R'(\eta)\frac{\xi^2}{\eta^2}]\, e^{-i\omega\tau}\, d\tau \tag{2.13}$$

where $\eta = \sqrt{\xi^2 + V_w^2\tau^2}$

$R(\cdot)$ = Von Karman correlation function of Eq. (2.6).

Using a standard integral (22) results in

$$\Phi(\xi,\omega) = \frac{2^{1/6}}{\Gamma(5/6)} [\mu^{5/6} K_{5/6}(\mu) - \tfrac{1}{2}\mu^{11/6} K_{1/6}(\mu)] \tag{2.14}$$

where $\mu = \sqrt{(\frac{\omega\xi}{V_w})^2 + (\frac{\xi}{aL})^2}$

$a = 1.339$ as in Eq. (2.4).

Note for $\omega \gg \frac{V_w}{aL}$ (i.e., in the inertial subrange)

$$\mu \to \frac{\omega\xi}{V_w} \tag{2.15}$$

The same dimensionless variable proposed by Davenport.

Figure 2.1 shows a comparison between the Von Karman form given by Eq. (2.14) and an exponential approximation

$$\Phi(\xi,\omega) \approx e^{-1.4\mu} \tag{2.16}$$

This approximation compares favorably with Davenport's model in the inertial subrange. At zero frequency, however, Davenport's model predicts perfect correlation for any spatial separation, a result at odds with Von Karman's model and with intuition.

Also shown in Figure 2.1 is the normalized cospectrum resulting from Dryden's (23) correlation function which is a simple exponential. Combining Eq. (2.16) and the Kaimel (24) spectral model results in the cross-spectrum for the longitudinal component

$$S(\xi,\omega) = \frac{\frac{2\sigma^2 L}{V_w} e^{-1.4\sqrt{(\frac{\omega\xi}{V_w})^2 + (\frac{\xi}{1.339L})^2}}}{1 + 1.572(\frac{\omega L}{V_w})^{5/3}} \tag{2.17}$$

where ξ is the separation distance in a plane normal to the mean wind. For many turbulence studies involving horizontal-axis wind turbines, the aerodynamic effects are largely determined by the longitudinal turbulent velocity component at points within the rotor disk plane. This plane is approximately normal to the mean wind direction. In this case, Eq. (2.17) provides an alternative model for these turbulence effects. It should be noted, however, that this model does not precisely account for the constraints imposed by the continuity of the fluid medium, while the Von Karman model does.

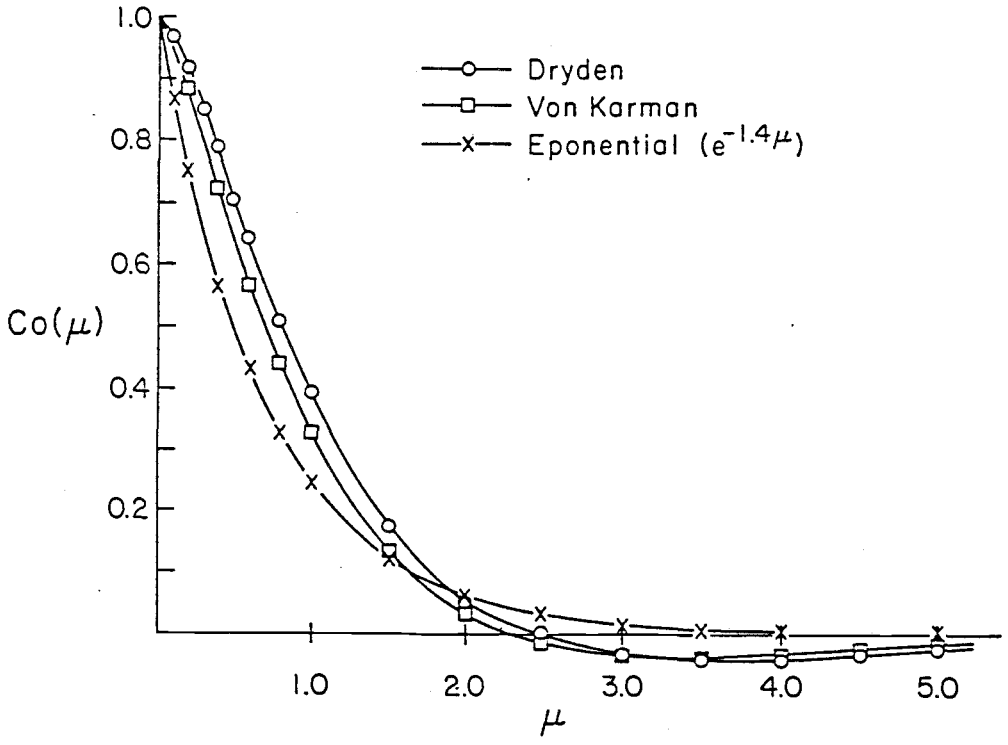

Figure 2.1. Three Models for the Turbulent Velocity Two-point Cospectrum

III. ATMOSPHERIC TURBULENCE INPUTS FOR HORIZONTAL AXIS WIND TURBINES

III.1 Introduction

In the previous chapter, models that give a statistical description of the turbulent fluctuations are presented. Even with a statistical model of the wind turbulence, there still remains the nontrivial task of computing the statistical response of a wind turbine for such atmospheric turbulence inputs. When it is desired to determine the dynamic response of a wind turbine for atmospheric inputs, it is necessary to find the aerodynamic forces and moments which are caused by the turbulence. This is no easy task since these forces and moments represent integrated effects along each of the wind turbine blades. These effects are further complicated by the fact that the turbulent velocity varies randomly across the rotor disk.

Considerable simplification is achieved by applying an approximation concept originally presented by Etkin (24), and further developed by Skelton (25) and by Holley and Bryson (26). In this approach, the spatial variation of the turbulence is approximated by a few terms in a series expansion. In particular for the work reported here, uniform terms across the disk, gradient terms which vary linearly across the disk, and the terms which vary quadratically across the disk are retained. Using linear aerodynamics, it is then possible to determine influence coefficients which give the forces

and moments for each of these time varying uniform, gradient, and quadratic terms. The computation of these coefficients is discussed in detail by Thresher et al. (27). Here we focus on determining a statistical model of the uniform, gradient, and quadratic terms which serve as excitations for the dynamic model of the wind turbine system.

III.2 Series Approximation to the Turbulent Velocity Field

The coordinate definitions used in this chapter are shown in Figure 3.1. In the vicinity of the wind turbine rotor disk, the turbulence velocity is expressed locally by the approximation

$$\begin{aligned}\hat{v}_i(x,z,t) = {} & V_i(t) + V_{i,x}(t)\,x + V_{i,z}(t)\,z \\ & + V_{i,xx}(t)\left(x^2 - \tfrac{1}{4}R^2\right) + V_{i,zz}(t)\left(z^2 - \tfrac{1}{4}R^2\right) \\ & + V_{i,zx}(t)\,zx + \text{higher order terms} \qquad (3.1)\end{aligned}$$

where R is the radius of the rotor disk.

In this approximation, the spatial randomness of the turbulence is accounted for by the time varying random quantities $V_i(t)$, $V_{i,x}(t)$, $V_{i,z}(t)$, $V_{i,xx}(t)$, $V_{i,zz}(t)$, $V_{i,zx}(t)$, and higher order terms. While this approximation appears to be a Taylor series expansion, it is not. Because of the random nature of the spatial variations, the samples from the statistical ensemble do not have the usual continuity and differentiability properties necessary for a true Taylor expansion. The expansion, however, can be thought of as a functional approximation. The series of functions:

$$f_0 = 1$$
$$f_1 = x$$
$$f_2 = z$$
$$f_3 = x^2 - 1/4\ R^2 \qquad (3.2)$$
$$f_4 = z^2 - 1/4\ R^2$$
$$f_5 = zx$$

were found by choosing polynomials with successively higher powers of x and z and enforcing conditions of mutual orthogonality over the rotor disk, i.e.,

$$\int f_j(x,z) f_k(x,z) dA = 0; \text{ for } j \neq k \qquad (3.3)$$

Here, the object is to choose the terms in the expansion so as to minimize some measure of the approximation error. When dealing with random functions, a reasonable error measure is its variance. It will be understood that convergence of the approximation series means that the error variance approaches zero as more and more terms are included. Convergence in variance further implies that the series converges in probability (28), i.e.,

$$\lim_{n\to\infty} \Pr\{|e_n| > \varepsilon\} = 0 \quad \text{for all } \varepsilon > 0 \qquad (3.4)$$

where e_n is the approximation error including only the nth order terms.

At any given time, the terms V_i, $V_{i,x}$, $V_{i,z}$, $V_{i,xx}$, $V_{i,zz}$, and $V_{i,zx}$ are chosen to minimize the criterion

$$\varepsilon = \frac{1}{A} \int_A \sum_i (\hat{v}_i - v_i)^2 dA \qquad (3.5)$$

where A = rotor disk area

$$\hat{v}_i = V_i + V_{i,x}x + V_{i,z}z + V_{i,xx}(x^2-\frac{1}{4}R^2)$$

$$+ V_{i,zz}(z^2-\frac{1}{4}R^2) + V_{i,zx}zx$$

$$v_i = v_i(x,z,t)$$

The necessary conditions for the minimization are

$$\frac{\partial \epsilon}{\partial V_i} = \frac{2}{A}\int_A (\hat{v}_i-v_i)\,dA = 0$$

$$\frac{\partial \epsilon}{\partial V_{i,x}} = \frac{2}{A}\int_A (\hat{v}_i-v_i)x\,dA = 0$$

$$\frac{\partial \epsilon}{\partial V_{i,z}} = \frac{2}{A}\int_A (\hat{v}_i-v_i)z\,dA = 0$$

$$\frac{\partial \epsilon}{\partial V_{i,xx}} = \frac{2}{A}\int_A (\hat{v}_i-v_i)(x^2-\frac{1}{4}R^2)dA = 0 \qquad (3.6)$$

$$\frac{\partial \epsilon}{\partial V_{i,zz}} = \frac{2}{A}\int_A (\hat{v}_i-v_i)(z^2-\frac{1}{4}R^2)dA = 0$$

$$\frac{\partial \epsilon}{\partial V_{i,zx}} = \frac{2}{A}\int_A (\hat{v}_i-v_i)(zx)\,dA = 0$$

which in turn require that

$$V_i(t) = \int(1)\, v_i(x,z,t)dA / \int(1)^2 dA$$

$$V_{i,x}(t) = \int x\, v_i(x,z,t)dA / \int x^2 dA$$

$$V_{i,z}(t) = \int z\, v_i(x,z,t)dA / \int z^2 dA \qquad (3.7)$$

$$V_{i,xx}(t) = \int(x^2 - \frac{1}{4}R^2)v_i(x,z,t)dA / \int(x^2 - \frac{1}{4}R^2)^2 dA$$

$$V_{i,zz}(t) = \int(z^2 - \frac{1}{4}R^2)^2 v_i(x,z,t)dA / \int(z^2 - \frac{1}{4}R^2)^2 dA$$

$$V_{i,zx}(t) = \int(zx)\, v_i\,(x,z,t)dA / \int(zx)^2 dA$$

Consider first the velocity component normal to the plane of the rotor disk, since it generally provides the most important aerodynamic effect on the wind turbine (29). In order to provide a more accurate determination of these effects, it is proposed to retain all terms including quadratic variations across the rotor disk of radius R. Thus, using Taylor's frozen field hypothesis relating the spatial and time dependency,

$$v_y(x,-V_w t,z) \approx V_y(t) + V_{y,x}(t)\, x + V_{y,z}(t)\, z + V_{y,xx}(t)\,(x^2 - \frac{1}{4}R^2) + V_{y,zz}(t)(z^2 - \frac{1}{4}R^2) + V_{y,zx}(t)\, zx \qquad (3.8)$$

Now, when the statistics of the terms $V_{y,zz}$ and $V_{y,xx}$ are considered it is found that the correlation between the terms exists which complicates the statistical modeling. To alleviate this problem, linear combinations of the last three terms are defined as follows:

$$V_{y,rr} = \frac{1}{2}(V_{y,zz} + V_{y,xx})$$

$$V_{y,rc} = \frac{1}{2}(V_{y,zz} - V_{y,xx})$$

$$V_{y,rs} = \frac{1}{2} V_{y,zx} \qquad (3.9)$$

Converting to polar coordinates and substituting Eq. (3.9) into Eq. (3.8) gives the following form for the series

$$v_y \tilde{=} V_y + V_{y,z}\, r\cos\theta + V_{y,x}\, r\sin\theta + V_{y,rr}\,(r^2 - \tfrac{1}{2}R^2) + V_{yrc}\, r^2\cos 2\theta + V_{y,rs}\, r^2 \sin 2\theta \qquad (3.10)$$

with the six relations:

$$V_y = \frac{1}{\pi R^2} \int_0^R \int_0^{2\pi} v_y \, r\,dr\,d\theta$$

$$V_{y,z} = \frac{4}{\pi R^4} \int_0^R \int_0^{2\pi} v_y (r\cos\theta)\, r\,dr\,d\theta$$

$$V_{y,x} = \frac{4}{\pi R^4} \int_0^R \int_0^{2\pi} v_y (r\sin\theta)\, r\,dr\,d\theta$$

$$V_{y,rr} = \frac{12}{\pi R^6} \int_0^R \int_0^{2\pi} v_y \,(r^2 - \tfrac{1}{2}R^2)\, r\,dr\,d\theta$$

$$V_{y,rc} = \frac{6}{\pi R^6} \int_0^R \int_0^{2\pi} v_y (r^2\cos 2\theta)\, r\,dr\,d\theta$$

$$V_{y,rs} = \frac{6}{\pi R^6} \int_0^R \int_0^{2\pi} v_y \,(r^2 \sin 2\theta)\, r\,dr\,d\theta$$

Note that the time argument has been dropped from these equations. It should be understood that these equations apply at any instant of time.

For the in-plane velocity components we retain only linear variations across the rotor disk. Since the in-plane components are only of secondary importance in calculating wind turbine rotor loads, it is felt that the considerable simplification afforded by neglecting the quadratic and higher order terms is justified. At this point, it is convenient to rearrange the gradient terms for the in-plane components. Certain combinations of the in-plane gradient terms always appear together in the linearized aerodynamic relations (30). Thus, the following terms are defined

$$\gamma_{zx} = \frac{1}{2}(V_{z,x} - V_{x,z}) \qquad \text{swirl}$$

$$\left.\begin{aligned} \bar{\gamma}_{zx} &= \frac{1}{2}(V_{z,x} + V_{x,z}) \\ \epsilon_{zx} &= \frac{1}{2}(V_{z,z} - V_{x,x}) \end{aligned}\right\} \qquad \text{shear strain rates}$$

$$\bar{\epsilon}_{zx} = \frac{1}{2}(V_{z,z} + V_{x,x}) \qquad \text{dilation} \qquad (3.12)$$

Typical fluid streamlines giving rise to positive terms are shown in Figure 3.2.

The two in-plane velocity components are thus approximated by:

$$v_x \approx V_x(t) + (\bar{\epsilon}_{zx}(t) - \epsilon_{zx}(t)) r \sin\theta$$

$$+ (\bar{\gamma}_{zx}(t) - \gamma_{zx}(t))\, r \cos\theta \qquad (3.13a)$$

$$v_z \simeq V_z(t) + (\bar{\gamma}_{zx}(t) + \gamma_{zx}(t))\, r \sin\theta + (\bar{\epsilon}_{zx}(t) + \epsilon_{zx}(t))\, r \cos\theta \tag{3.13b}$$

Now, if the statistics of the turbulence field are known, it is then possible to utilize Eqs. (3.10) and (3.13) to compute the correlation statistics or power spectral densities among the twelve turbulent terms. As an example, consider the autocorrelation function for the uniform, through-the-disk term V_y. Direct application of the first of Eqs. (3.11) gives

$$R_{V_y}(\tau) \triangleq E[V_y(t+t)\, V_y(t)] \tag{3.14a}$$

$$= \frac{1}{A^2} \int_A \int_A E[v_y(r,\theta,t+\tau)\, v_y(\rho,\phi,t)]\, dA_1 dA_2 \tag{3.14b}$$

Using Taylor's hypothesis yields

$$R_{V_y}(\tau) = \frac{1}{A^2} \int_A \int_A R_{yy}(\vec{\xi} - \vec{V}_w \tau)\, dA_1 dA_2 \tag{3.15}$$

where $R_{yy}(\cdot)$ = correlation function of the v_y component for the separation vector argument

$$\vec{\xi} - \vec{V}_w \tau = \begin{cases} r\sin\theta - \rho\sin\phi \\ -V_w \tau \\ r\cos\theta - \rho\cos\phi \end{cases}$$

$$dA_1 = r\, dr\, d\theta$$

$$dA_2 = \rho\, d\rho\, d\phi$$

r, θ = polar coordinates in disk 1

ρ, ϕ = polar coordinates in disk 2.

Fourier transforming Eq. (3.15) yields an expression for the power spectral density

$$S_{V_y}(\omega) \triangleq \int_{-\infty}^{\infty} R_{V_y}(\tau) e^{-i\omega\tau} \, d\tau \tag{3.16a}$$

$$= \frac{1}{A^2} \int_A \int_A S_{yy}(\vec{\xi}, \omega) \, dA_1 dA_2 \tag{3.16b}$$

where $S_{yy}(\vec{\xi}, \omega)$ is the two point, cross-spectral density defined by Eq. (2.9). This power spectral density can be computed in two ways depending on which model for the turbulence is utilized. First, using the isotropic, Von Karman model from Eq. (2.8) with the power spectral density expression of Eq. (3.16b) yields

$$S_{V_y}(\omega) = \int_{-\infty}^{\infty} \left\{ \frac{1}{A^2} \int_A \int_A \left[R(\eta) + \frac{1}{2} \eta R'(\eta) \frac{\xi^2}{\eta^2} \right] dA_1 dA_2 \right\} e^{-i\omega\tau} \, d\tau \tag{3.17}$$

where

$$\eta^2 = \xi^2 + (V_w \tau)^2$$

$$\xi^2 = (r \cos\theta - \rho \cos\phi)^2 + (r \sin\theta - \rho \sin\phi)^2$$

$$= r^2 + \rho^2 - 2r\rho \cos(\theta - \phi)$$

and $R(\cdot)$ = Von Karman correlation function in Eq. (2.6). Second, the modified Davenport-Kaimal model is used for the cross-spectrum giving

$$S_{V_y}(\omega) = \frac{1}{A^2} \int_A \int_A S(\xi,\omega)\, dA_1 dA_2 \qquad (3.18)$$

where $S(\xi,\omega)$ is given by EQ. (2.17)

and $\xi^2 = r^2 + \rho^2 - 2r\rho \cos(\theta-\phi)$ as before. Because of the complexity of the double area integrals of Eqs. (3.17) and (3.18), numerical procedures outlined in Appendix A are used to compute the results. The resulting power spectral density functions depend upon the turbulence parameters σ and L, the mean wind speed V_w, and the rotor disk radius, R. However, by using appropriate nondimensional forms in Table 3.1, the power spectral density $S_{V_y}(\omega)$, can be reduced to a single parameter family of curves. In particular,

$$\frac{\omega S_{V_y}(\omega)}{\sigma^2} = f\left(\frac{L}{V_w}, \frac{R}{L}\right) \qquad (3.19)$$

Figures 3.3 and 3.4 show the resulting curves for the two values of R/L representing typical wind turbines at 8 KW and 2.5 MW respectively.

Besides the isotropic, Von Karman, and the modified Davenport-Kaimal model results, Figures 3.3 and 3.4 show the results for two other models. In the isotropic, Dryden model, the correlation function in Eq. (3.17) is given by the simple exponential

$$R(\eta) = \sigma^2 e^{-\eta/L} \qquad (3.20)$$

In the Fichtl model (31), an alternative approach to Eq. (3.17) is utilized. Fichtl obtained an analytical expression for the dimensionless spectrum

$$\frac{\omega S_{V_y}(\omega)}{\sigma^2} = 2\left(\frac{\omega L}{V_w}\right)\left\{\frac{1}{1+\left(\frac{\omega L}{V_w}\right)^2} - \frac{1+\left(\frac{\omega L}{V_w}\right)^2 + 2\left(\frac{\Pi L}{2R}\right)^2}{\left[1+\left(\frac{\omega L}{V_w}\right)^2 + \left(\frac{\Pi L}{2R}\right)^2\right]^2}\right\} \qquad (3.21)$$

Examination of Figures 3.3 and 3.4 shows that Fichtl's result compares quite favorably with the numerical integration of Eq. (3.17) using the Dryden model.

Using methods analogous to those just given, the spectra for other terms in the expansion can be determined. Particularly interesting, is the case of the vertical gradient of the longitudinal velocity component, $V_{y,z}$. This term acts like a time varying wind shear across the rotor disk. Using the necessary conditions for minimum approximation error in Eq. (3.11), the following result for the isotropic case is obtained.

$$S_{V_{y,z}}(\omega) = \int_{-\infty}^{\infty} \left(\frac{4}{\Pi R^4}\right)^2 \int_A \int_A r\rho\cos\theta\,\cos\phi\,\left[R(\eta)+\frac{1}{2}\eta R'(\eta)\frac{\xi^2}{\eta^2}\right] dA_1\,dA_2\, e^{-i\omega\tau}\,d\tau \qquad (3.22)$$

for the modified Davenport-Kaimal case

$$S_{V_{y,z}}(\omega) = \left(\frac{4}{\Pi R^2}\right)^2 \int_A \int_A r\rho\cos\theta\,\cos\phi\; S(\xi,\omega)\; dA_1\,dA_2 \qquad (3.23)$$

and for Fichtl's integration of the Dryden model

$$\frac{R^2\omega S_{V_{y,z}}(\omega)}{\sigma^2} = 2\left(\frac{R}{L}\right)^2\left(\frac{\omega L}{V_w}\right)\left[\frac{1+\left(\frac{\omega L}{V_w}\right)^2}{1+\left(\frac{\omega L}{V_w}\right)^2+\left(\frac{\pi L}{2R}\right)^2}\right.$$

$$\left. + \ln\left(\frac{1+\left(\frac{\omega L}{V_w}\right)^2+\left(\frac{\pi L}{2R}\right)^2}{1+\left(\frac{\pi L}{2R}\right)^2}\right) - \frac{1}{2}\frac{\left(\frac{\pi L}{2R}\right)^4}{\left[1+\left(\frac{\omega L}{V_w}\right)^2+\left(\frac{\pi L}{2R}\right)^2\right]^2}-1\right]$$

(3.24)

Results in dimensionless form for numerical integrations of Eqs. (3.22) and (3.23) are compared to Eq. (3.24) in Figures 3.5 and 3.6. Here, a much larger divergence among the various models can be observed. For the smaller 8 kW turbine (Figure 3.5), the low frequency portion of the spectrum for the modified Davenport-Kaimal model is approximately five times that of the other models. This may be explained by considering the spectra shown in Figure 2.1. The velocity gradient term is determined by the velocity difference across the rotor disk. For a small wind turbine, the separation is small so that the small μ portion of the curve is dominant. In this region the exponential curve is significantly below the Dryden and Von Karman curves. Thus, the turbulent velocity at points with small separation will be less correlated for the exponential model, and the expected difference between the velocities at the two points will be larger. This leads to a significant overestimation of the low frequency, spectral density for the gradient term in the modified Davenport-Kaimal case. Among the remaining three models, only the Von Karman model properly represents the -5/3 power law for the high

frequency turbulence spectra. This accounts for the difference at high frequency between the Dryden and Von Karman results in Figure 3.6. Fichtl's model gives a much sharper high frequency cut-off than the theory using Eq. (3.22). For these reasons, the Von Karman model will be adopted in the remaining computations of the other turbulence input terms.

Retaining the uniform, gradient, and quadratic terms in the approximation results in the following twelve terms which vary randomly with time: V_x, V_y, V_z, $V_{y,x}$, $V_{y,z}$, γ_{zx}, $\bar{\gamma}_{zx}$, ϵ_{zx}, $\bar{\epsilon}_{zx}$, $V_{y,rr}$, $V_{y,r\theta}$, and $V_{y,r\theta}$. The correlation statistics for these twelve terms are further described in section III.4.

III.3 Error Discussion for the Local Approximation of the Turbulence Field

It is desirable to estimate the amount of error introduced by truncating the higher order terms in the local approximation to the turbulence field given by Eq. (3.1). Since the velocity component through the rotor disk, v_y, produces the greatest aerodynamic forces, consider the error variance produced by the approximation of this component

$$\epsilon_1(r,\theta) = \frac{1}{\sigma^2} E[(\hat{v}_y(r,\theta,t) - v_y(r,\theta,t))^2] \tag{3.25}$$

Averaging over the rotor disk gives

$$\bar{\epsilon}_1 = \frac{1}{A} \int_A \epsilon_1(r,\theta) dA \tag{3.26}$$

Using the relations for terms $V_y(t)$, $V_{y,x}(t)$, and $V_{y,z}(t)$ given by Eqs. (3.11) yields the useful relation

$$\int_A (\hat{v}_y - v_y)\, \hat{v}_y \, dA = 0 \tag{3.27}$$

and hence

$$\bar{\varepsilon}_1 = \frac{1}{A\sigma^2} \int_A E[v_y^2]\,dA - \frac{1}{A\sigma^2} \int_A E[\hat{v}_y v_y]\,dA$$

$$= 1 - \frac{1}{\sigma^2} E[V_y^2] - \frac{I_x}{A\sigma^2} E[V_{y,x}^2] - \frac{I_z}{A\sigma^2} E[V_{y,z}^2] \tag{3.28}$$

where $I_x = I_z = \frac{\pi R^4}{4}$ the area moments about the x and z axes which finally gives

$$\bar{\varepsilon}_1 = 1 - \frac{R_{V_y}(0)}{\sigma^2} - \frac{1}{4}\frac{R^2 R_{V_{y,x}}(0)}{\sigma^2} - \frac{1}{4}\frac{R^2 R_{V_{y,z}}(0)}{\sigma^2} \tag{3.29}$$

where the notation $R_{sub}(\cdot)$ denotes the autocorrelation function for the subscript random variable and $R_{sub}(0)$ is the variance. This quantity, $\bar{\varepsilon}_1$, can be interpreted as a measure of the total variance of the part of the turbulent velocity that is not included in the model. Thus, the averaged error, $\bar{\varepsilon}_1$ is zero if the approximation is perfect, and $\bar{\varepsilon}_1 = 1$ if the trivial approximation $\hat{v}_y = 0$ is used.

In a similar fashion, the quantity $\bar{\varepsilon}_0$ can be defined when only the uniform terms are retained, and $\bar{\varepsilon}_2$ when uniform, gradient, and quadratic terms are retained. Table 3.2 shows the relative approximation error for the series approximation. The relative approximation error is seen to depend on the dimensionless parameter R/L where R is the disk radius and L is the turbulence integral scale. The

computation was carried out using the three dimensional Von Karman correlation function for isotropic turbulence.

Observing the results given in Table 3.2, a significant improvement is obtained when the gradient terms, $V_{y,x}$ and $V_{y,z}$, are included along with the uniform term V_y. However, only a small further improvement is obtained when the quadratic terms are also included. This leads to the conclusion that the unmodeled portion of the turbulence is highly disorganized and probably has a negligible effect on the forces and moments felt at the hub.

Table 3.1. Scaling Parameters for Nondimensional Curves

Variables	Scaling Parameters
Turbulent velocity, V_i	σ
Velocity gradient, $V_{i,j}$	σ/R
Velocity quadratic, $V_{i,jk}$	σ/R^2
Frequency, ω	$V_{w/L}$

Table 3.2. Relative Approximation Error for Series Approximation

R/L	$\bar{\epsilon}_0$	$\bar{\epsilon}_1$	$\bar{\epsilon}_2$
.01	.044	.026	.020
.054	.135	.081	.060
.1	.201	.121	.091
.3	.397	.250	.189
.5	.527	.348	.264
1.0	.724	.527	.411
2.0	.889	.737	.608

III.4 Filtered Noise Model for the Turbulence

Retaining the uniform, gradient, and quadratic terms in the local approximation of the turbulent velocity field given by Eq. (3.1), results in twelve time varying input terms which can excite the wind turbine system. To characterize the response of the wind turbine for these excitations it is necessary to find all of the auto and cross spectra for these inputs. Section III.2 outlines the procedure for this computation which involves two disk area integrations. To avoid having to compute these integrals for every case desired, it is useful to compute approximate models which can be used to analytically generate the required spectra.

Consider a dynamic system of the general form

$$\frac{dx}{dt} = Ax + Bw \tag{3.30}$$

where x is the vector of system states

w is the vector of independent white noise excitations

A, B are matrices.

The state correlation matrix is defined by

$$R(\tau) = E\left[x(t+\tau)x^T(t)\right] \tag{3.31}$$

and is computed from the differential equation (for $\tau \geq 0$)

$$\frac{d}{d\tau}R = AR, \qquad R(0) = X \tag{3.32}$$

where the covariance matrix X (assuming zero mean) is given by the solution to the Lyapunov equation (32)

$$AX + XA^T + BS_w B^T = 0 \tag{3.33}$$

and S_w is the diagonal matrix of noise power spectral densities.

Given the correlation matrix $R(\tau)$, the matrix A can be computed by integrating Eq. (3.32)

$$R(\infty) - R(0) = A \int_0^\infty R(\tau)d\tau \tag{3.34}$$

or

$$A = -X[S_+]^{-1} \tag{3.35}$$

where $S_+ = \int_0^\infty R(\tau)d\tau$

$x = R(0)$

and $R(\infty) = 0$.

The B matrix then must satisfy Eq. (3.33) so that

$$BS_wB^T = -(AX+XA^T) \tag{3.36}$$

If the noise terms are chosen (for simplicity) to have identical power spectral densities, then

$$BB^T = -\frac{1}{S_w}(AX+XA^T) \tag{3.37}$$

where S_w is now the scalar power spectral density of each noise excitation. A unique matrix B can be determined if it is also required to be triangular, the result of which is called the Cholesky square root matrix (33). Appendix B gives the procedure for Cholesky decomposition.

In cases where $R(\tau)$ is diagonal, considerable simplification results. In this case, A and B will both be diagonal and the resulting scalar equations apply:

$$A_K = -\frac{X_K}{S_{+K}} \tag{3.38}$$

$$B_K = \sqrt{-\frac{2A_K X_K}{S_w}} \tag{3.39}$$

where the subscript indicates the kth diagonal element.

It is convenient to choose noise power spectral density

$$S_w = \frac{\sigma^2 L}{V_w^3} \tag{3.40}$$

thereby defining the noise vector to be dimensionless. Also, dimensionless parameters can be chosen so that

$$a_* = -\frac{L\,A_K}{V_w} \tag{3.41}$$

$$b_* = \begin{cases} \dfrac{L\,B_K}{V_w^2} & \text{for uniform terms} \\ \dfrac{RL\,B_K}{V_w^2} & \text{for shear terms} \\ \dfrac{R^2 L\,B_K}{V_w^2} & \text{for quadratic terms} \end{cases} \tag{3.42}$$

These parameters only depend on the dimensionless ratio R/L, where again R is the disk radius and L is the turbulence integral scale. As an example of the computational procedure, consider the turbulence component V_y. In this case,

$$\frac{R_{V_y}(0)}{\sigma^2} = \frac{1}{A^2} \iint_{A\,A} g(\frac{\xi}{L},0)\,dA_1\,dA_2 \tag{3.43}$$

and

$$\frac{\dot{V}_w S + V_y \tau(0)}{L\sigma^2} = \frac{1}{A^2} \int_0^\infty \iint_{A\,A} (\frac{V_w}{L})\, g(\frac{\xi}{L},\frac{V_w\tau}{L})\,dA_1\,dA_2\,d\tau \tag{3.44}$$

where $g(\frac{\xi}{L},\frac{V_w\tau}{L})$ = nondimensional velocity correlation function

$$= \frac{1}{\sigma^2} R_{yy}(\vec{\xi}-\vec{V}_w\tau)$$

$$\xi = |\vec{\xi}| = r^2 + \rho^2 - 2r\rho\,\mathrm{Cos}(\theta-\phi)$$

$$dA_1 = r\,dr\,d\theta$$

$$dA_2 = \rho\,d\rho\,d\phi$$

For the Von Karman correlation model

$$g(\frac{\xi}{L},\frac{V_w\tau}{L}) = \frac{1}{\sigma^2}\left[R(\eta) + \frac{1}{2}\eta R'(\eta)\frac{\xi^2}{\eta^2}\right] \tag{3.45}$$

where $\eta = \sqrt{\xi^2 + V_w^2\tau^2}$

$R(\cdot)$ = Von Karman correlation function of Eq. (2.6). The integrals given by Eqs. (3.43) and (3.44) were computed numerically for several values of R/L and results are given in Table 3.3. The results of a_* and b_* for V_y are also plotted in Figures 3.7 and 3.8.

Using similar procedures, the dimensionless parameters for all twelve of the turbulence input terms can be computed. However, before presenting these results, consider the effects of the symmetry due to the assumed isotropy of the turbulence field. The statistics of several pairs of the input terms are the same; namely (V_z, V_x), ($V_{y,z}$, $V_{y,x}$), (ϵ_{zx},$\bar{\gamma}_{zx}$), and finally ($V_{y,rs}$, $V_{y,rc}$).

So far we have discussed only the autocorrelation characteristics of the various terms in the velocity field approximation. What about the cross-correlation characteristics? Fortunately, due to the assumed isotropy of the model and the orthogonality properties of the functions f_0, f_1..., f_5 in Eqs.(3.2), most of the twelve terms in the velocity approximation are entirely uncorrelated. It turns out that there is a small correlation between V_y and $V_{y,rr}$ and a more important relation between V_y and in-plane dilation term, $\bar{\epsilon}_{zx}$ (34). This later relation can be derived by considering the constraint of conservation of mass flowing into rotor disk. Equating the mass flowing into and out of a finite thickness rotor disk and then letting the thickness go to zero gives

$$\frac{\partial}{\partial y}\int_A \rho v_y dA + \int_0^{2\pi} \rho R(v_x \sin\phi + v_z \cos\phi)\, d\phi = 0 \qquad (3.46)$$

Substituting the approximations for v_x, v_y, and v_z from Eqs. (3.8) and (3.13), using Taylor's frozen field hypothesis, and assuming incompressible flow gives the result

$$\frac{d}{dt} V_y = 2V_w \bar{\epsilon}_{zx} \tag{3.47}$$

It should be remembered that V_y, $\bar{\epsilon}_{zx}$, etc. are functions of time only. If the continuity equation is applied directly in differential form to the approximation velocity relations then the $V_{y,rr}$ term also appears in the resulting relation. This result may explain the small correlation observed between V_y and $V_{y,rr}$ numerically.

Here, we consider two models. First, all twelve of the turbulence terms are assumed to be mutually uncorrelated which simplifies the model considerably. Thus, each of the white noise excitation terms can be considered to be independent, resulting in 12 decoupled stochastic differential equations of the form Eq. (3.30) in the first order case. So there are only eight independent sets of parameters. For any specific case, a total of 16 a_* and b_* dimensionless parameters along with V_w, σ, L and R will specify the turbulence model completely. Tables 3.4, 3.5, 3.6, 3.7, 3.8, 3.9, and 3.10 give the remaining seven sets of dimensionless parameters. Second, since V_y, $\bar{\epsilon}_{zx}$, and $V_{y,rr}$ are correlated, we assume a third order coupled stochastic differential equation of the form

$$\frac{dx}{dt} = A_* x + B_* w \tag{3.48}$$

where $x = [V_y, \bar{\varepsilon}_{zx}, V_{y,rr}]^T$

w is the vector of independent white noise excitations

A_* and B_* are 3x3 matrices

and that the result of the turbulence terms are mutually uncorrelated. Tables 3.15 and 3.16 give the dimensionless parameters of the third order model for V_y, $\bar{\varepsilon}_{zx}$, and $V_{y,rr}$. Table 3.11 gives the dimensionless variance between $V_{y,rr}$ and V_y. Tables 3.12, 3.13, and 3.14 give the dimensionless S_+ for V_y, $\bar{\varepsilon}_{zx}$, and $V_{y,rr}$ respectively.

In order to avoid the inconvenient interpolation necessary in evaluating the model parameters when R/L is not a tabulated value, a regression procedure was utilized to give a formula for calculating the dimensionless parameters. The standard linear regression procedure is outlined in Appendix C.

For the uniform terms, V_y, V_x, and V_z, the following form was found to describe the data:

$$a_* \text{ or } b_* = k_1 - \frac{k_2 R_* (1+k_3 R_*)}{1 + k_4 R_*} \tag{3.49}$$

where $R_* = R/L$.

The parameters k_1, k_2, k_3, and k_4 are determined as follows:

1. k_1 is given by the limit as $R_* \to 0$ which is either 1, 2 or $\sqrt{2}$.
2. Assuming $k_3 = 0$ and R_* is small, Eq. (3.49) can be rearranged so that

$$a_* \text{ or } b_* \approx k_1 - k_2 R_* + k_2 k_4 R_*^2 \tag{3.50}$$

the parameters k_2 and k_4 can be found using standard linear regression based on the data for small R_*.

3. The equation is then rearranged into the form

$$a_* \text{ or } b_* = k_1 + c_1 \frac{k_4 R_*}{1+k_4 R_*} + c_2 R_* \qquad (3.51)$$

and the parameters c_1 and c_2 are again determined using standard linear regression with k_1 and k_4 fixed. These values then give the final values of the k_2 and k_3 parameters.

Table 3.17 shows the resulting regression parameters for the uniform turbulence terms including the in-plane velocity components.

For the shear and quadratic terms a different form was found to fit the data. In this case,

$$a_* \text{ or } b_* = k_1 R_*^{-k_2} + k_3 + k_4 R_* \qquad (3.52)$$

The parameter k_2 was chosen to match the shape of a log-log plot of a_* or b_* vs. R_* (Figures 3.9 and 3.10). A value of $k_2 = 1$ was found to give good results for a_* and $k_2 = 1/4$ for b_*. The remaining parameters, k_1, k_3, and k_4, were determined by standard linear regression. Table 3.18 gives the resulting values for both the normal and in-plane components for the shear terms and for the normal component quadratic terms.

Finally, in the case of the third order model for V_y, $\bar{\epsilon}_{zx}$, and $V_{y,rr}$ another form was found to fit most of the elements of A_* and B_* matrices except a_{12*} and a_{23*}. In this case,

$$a_{ij*} \text{ or } b_{ii*} = k_1 R_*^{k_2} (k_3+R_*)^{k_4} \tag{3.53}$$

and $$a_{23*} = R_*^{-1.13}(0.257 - 0.082\ R_* - 0.01 R_*^2) \tag{3.54}$$

$$a_{12*} = \frac{2}{R_*} \tag{3.55}$$

where $i = 2,3$ and $j = 1,2$, and 3 which stand for V_y, $\bar{\epsilon}_{zx}$, and $V_{y,rr}$ respectively.

The rest of the elements of A_* and B_* are equal to zero. Table 3.19 gives the resulting regression parameters for the third order model. In all cases the maximum deviation of the data from the regression curves was less than 5%.

One of the desirable properties of the approximate filtered noise model is the ease with which either the correlation function or the power spectral density can be computed. Once a_* and b_* are determined, the autocorrelation function for the filtered response is exponential (35) and is given by

$$R_x(\tau) = \sigma^2 \left(\frac{b_*^2}{2a_*}\right) e^{-\left|\frac{a_* V_w \tau}{L}\right|} \tag{3.56}$$

and from Eq. (3.16a)

$$S_x(\omega) = \frac{\left(\frac{b_* V_w}{L}\right)^2 \left(\frac{\sigma^2 L}{V_w}\right)}{\left(\frac{a_* V_w}{L}\right)^2 + \omega^2} \tag{3.57}$$

where ω is the radian frequency. These equations are appropriate for the case of the uniform velocity components. Since the gradient and quadratic terms have different dimensions involving length in the denominator, b_* in Eqs. (3.56) and (3.57) should be replaced by b_*/R and b_*/R^2 for the gradient and quadratic terms respectively.

III.5 Summary of the Turbulence Model

$$v_y(x,-V_w\tau,z) \approx V_y(t) + V_{y,z}(t)\,z + V_{y,x}(t)\,x + V_{y,rr}(t)(z^2+x^2-\tfrac{1}{2}R^2) + V_{y,rc}(t)(z^2-x^2) + V_{y,rs}(t)\,(2zx) \qquad (3.58)$$

In-plane velocity components:

$$v_x(x,-V_w\tau,z) \approx V_x(t) + (\bar{\epsilon}_{zx}(t) - \epsilon_{zx}(t))x + (\bar{\gamma}_{zx}(t) - \gamma_{zx}(t))z$$

$$v_z(x,-V_w\tau) \approx V_z(t) + (\bar{\gamma}_{zx}(t) + \gamma_{zx}(t))x + (\bar{\epsilon}_{zx}(t) + \epsilon_{zx}(t))z \qquad (3.59)$$

For the first order model, each of the turbulence terms is given by an equation of the form

$$\frac{d}{dt}(V_{sub}) + \left(\frac{V_w a_*}{L}\right) V_{sub} = \left(\frac{V_w^2 b_*}{R^n L}\right) w_k \qquad (3.60)$$

where the notation V_{sub} denotes one of the 12 turbulence terms and a_* and b_* are given by regression Eqs. (3.49) or (3.52) which depend on the ratio R/L. The n power of R is 0, 1, or 2 depending on whether the term is a uniform, shear, or quadratic term, respectively. The noise term w_k for each of the 12 turbulence terms is an independent noise source with PSD = $\frac{\sigma^2 L}{V_w^3}$. The uncorrelated model has the following form:

$$\dot{x} = Ax + Bw \tag{3.61}$$

where $x = [V_x V_y V_z \; V_{y,x} \; V_{y,z} \; \gamma_{zx} \; \bar{\gamma}_{zx} \; \epsilon_{zx} \; \bar{\epsilon}_{zx} \; V_{y,rr} \; V_{y,rc} \; V_{y,rs}]$

w = 12x1 vector of dimensionless, white noise excitations

A and B are diagonal matrices.

For the third order model, the turbulence terms of V_x, $\bar{\epsilon}_{zx}$, and $V_{y,rr}$ are given by an equation of the form

$$\dot{x} = A_* x + B_* w \tag{3.62}$$

where $x = [V_y \bar{\epsilon}_{zx} \; V_{y,rr}]^T$

w is the vector of independent white noise excitations

A and B are 3x3 matrices whose elements are given by Eqs. (3.53), (3.54), and (3.55).

The rest of the turbulence terms have the same form as Eq. (3.60). The correlated model has the following form:

$$\dot{x} = Ax + Bw \tag{3.63}$$

where $x = [V_y \; \bar{\varepsilon}_{zx} \; V_{y,rr} \; V_x \; V_z \; V_{y,x} \; V_{y,z} \; \gamma_{zx} \; \bar{\gamma}_{zx} \; \varepsilon_{zx} \; V_{y,rc} \; V_{y,rs}]$

w = 12x1 vector of dimensionless, white noise excitations

$$A = \begin{bmatrix} 0 & a_{12} & 0 & & & & & & & & & \\ a_{21} & a_{22} & a_{23} & & & & & & & & & 0 \\ a_{31} & a_{32} & a_{33} & & & & & & & & & \\ & & & a_{44} & & & & & & & & \\ & & & & \ddots & & & & & & & \\ & & & & & \ddots & & & & & & \\ & & & & & & \ddots & & & & & \\ & & 0 & & & & & & & & & a_{1212} \end{bmatrix}$$

$$B = \begin{bmatrix} 0 & 0 & 0 & & & & & & & & & \\ 0 & b_{22} & 0 & & & & & & & & & 0 \\ 0 & 0 & b_{33} & & & & & & & & & \\ & & & b_{44} & & & & & & & & \\ & & & & \ddots & & & & & & & \\ & & & & & \ddots & & & & & & \\ & & & & & & \ddots & & & & & \\ & & 0 & & & & & & & & & b_{1212} \end{bmatrix}$$

Table 3.3. Dimensionless Parameters for V_y Turbulence Term

$\frac{R}{L}$	$\frac{X}{\sigma^2}$	$\frac{2V_w S_+}{L\sigma^2}$	a_*	b_*
.01	.95582	1.9984	.95659	1.3523
.054	.86522	1.9795	.87418	1.2299
.1	.79881	1.9489	.81975	1.1444
.3	.60298	1.7664	.68272	.90738
.5	.47315	1.5636	.60521	.75678
1	.27623	1.0876	.50796	.52974
2	.11139	.52751	.42233	.30673

Table 3.4. Dimensionless Paremeters for V_x and V_z Turbulence Terms

$\frac{R}{L}$	$\frac{X}{\sigma^2}$	$\frac{2V_w S_+}{L\sigma^2}$	a_*	b_*
.01	.96133	1.0000	1.9227	1.9227
.054	.88192	.99055	1.7807	1.7723
.1	.82350	.97526	1.6888	1.6678
.3	.64926	.88402	1.4689	1.3811
.5	.53105	.78262	1.3571	1.2006
1	.34405	.55790	1.2334	.92124
2	.17081	.29557	1.1558	.62837

Table 3.5. Dimensionless Parameters for $V_{y,x}$ and $V_{y,z}$ Turbulence Terms

$\frac{R}{L}$	$\frac{R^2X}{\sigma^2}$	$\frac{2V_w R^2 S_+}{L\sigma^2}$	a_*	b_*
.01	.035906	.0021592	33.259	1.5455
.054	.10855	.032733	6.6325	1.2000
.1	.15982	.082957	3.8531	1.1098
.3	.29302	.34987	1.6750	.99077
.5	.35785	.60333	1.1863	.92141
1	.39306	1.0108	.77774	.78192
2	.30357	1.1189	.54262	.57398

Table 3.6. Dimensionless Parameters for γ_{zx} Turbulence Terms

$\frac{R}{L}$	$\frac{R^2X}{\sigma^2}$	$\frac{2V_wR^2S_+}{L\sigma^2}$	a_*	b_*
.01	.024526	.0011063	44.339	1.4748
.054	.074256	.016539	8.9795	1.1548
.1	.10954	.041511	5.2776	1.0753
.3	.20291	.17427	2.32869	.97213
.5	.25068	.30000	1.67120	.91535
1	.28412	.50000	1.13648	.80361
2	.23440	.54242	.86427	.63653

Table 3.7. Dimensionless Parameters for $\bar{\gamma}_{zx}$ and ϵ_{zx} Turbulence Terms

$\frac{R}{L}$	$\frac{R^2X}{\sigma^2}$	$\frac{2V_wR^2S_+}{L\sigma^2}$	a_*	b_*
.01	.015714	.0005748	54.676	1.1309
.054	.047626	.0084934	11.215	1.0336
.1	.070353	.021155	6.6512	.96740
.3	.13125	.087563	2.9978	.88709
.5	.16345	.15081	2.1676	.84178
1	.18939	.25267	1.4991	.75347
2	.16411	.27963	1.1738	.62069

Table 3.8. Dimensionless Parameters for $\bar{\epsilon}_{xz}$ Turbulence Terms

$\frac{R}{L}$	$\frac{\bar{R}^2 X}{\sigma^2}$	$\frac{2V_w R^2 S_+}{L\sigma^2}$	a_*	b_*
.01	.0069021	.0000829	166.52	1.5162
.054	.020995	.0013246	31.700	1.1537
.1	.031162	.0035154	17.729	1.0512
.3	.059582	.016089	7.4158	.94005
.5	.076227	.027527	5.5384	.95281
1	.094673	.039491	4.7946	.95281
2	.093809	.034137	5.4961	1.0155

Table 3.9. Dimensionless Parameters for $V_{y,rr}$ Turbulence Terms

$\frac{R}{L}$	$\frac{R^4 X}{\sigma^2}$	$\frac{2 R^4 V_w S_+}{L\sigma^2}$	a_*	b_*
.01	.025951	.0004757	109.13	2.3800
.054	.079814	.0078960	20.216	1.7964
.1	.12014	.021981	10.931	1.6207
.3	.24508	.13285	3.6896	1.3448
.5	.33273	.29452	2.2595	1.2262
1	.46242	.76550	1.2081	1.0570
2	.50905	1.4625	.69615	.84188

Table 3.10. Dimensionless Parameters for $V_{y,rs}$ and $V_{y,rc}$ Turbulence Terms

$\frac{R}{L}$	$\frac{R^4 X}{\sigma^2}$	$\frac{2 R^4 V_w S_+}{L\sigma^2}$	a_*	b_*
.01	.013089	.00024211	108.13	1.6824
.054	.040257	.0040190	20.033	1.2700
.1	.060600	.011189	10.832	1.1458
.3	.12364	.067636	3.6560	.95081
.5	.16791	.15002	2.2386	.86705
1	.23367	.39047	1.1969	.74789
2	.25844	.74662	.69230	.59820

Table 3.11. Dimensionless Variance between $V_{y,rr}$ and V_y Turbulence Terms

$\frac{R}{L}$	$\frac{R^2X}{\sigma^2}$
0.01	-0.0151678
0.054	-0.0456605
0.1	-0.0669269
0.3	-0.1199101
0.5	-0.1425811
1.0	-0.1448530
2.0	-0.0911425

Table 3.12. Dimensionless S_+ between $\bar{\varepsilon}_{zx}$ and V_y Turbulence Terms

$\frac{R}{L}$	$\frac{2V_wRS_+}{L\sigma^2}$
0.01	-0.00913405
0.054	-0.047092884
0.1	-0.080925338
0.3	-0.186398049
0.5	-0.296933816
1.0	-0.296933816
2.0	-0.242274579

Table 3.13. Dimensionless S_+ between $\bar{\epsilon}_{zx}$ and $V_{y,rr}$ Turbulence Terms

$\frac{R}{L}$	$\frac{2V_w R^3 S_+}{L\sigma^2}$
0.01	0.0001876244
0.054	0.0030932480
0.1	0.008490465
0.3	0.0472647
0.5	0.09684195
1.0	0.21528977
2.0	0.33226495

Table 3.14. Dimensionless S_+ between $V_{y,rr}$ and V_y Turbulence Terms

$\frac{R}{L}$	$\frac{2V_w R^2 S_+}{L\sigma^2}$
0.01	-0.000935167
0.054	-0.0151960
0.1	-0.0383445
0.3	-0.160252
0.5	-0.269937
1.0	-0.423823
2.0	-0.398774

Table 3.15. Dimensionless Parameters for A_* Matrix Components (3rd Order Model)

$\frac{R}{L}$	a_{21*}	a_{22*}	a_{23*}	a_{31*}	a_{32*}	a_{33*}
0.01	-0.70115	-151.18	46.825	-0.8596	-177.60	-54.168
0.054	-0.53921	-29.058	6.802	-0.691	-27.027	-13.094
0.1	-0.50086	-13.820	3.3342	-0.55644	-13.930	-7.8350
0.3	-0.47872	-5.4769	0.90543	-0.63316	-4.6978	-3.1841
0.5	-0.50170	-3.8562	0.47358	-0.63777	-3.0056	-2.1165
1.0	-0.60054	-2.6130	0.16196	-0.65365	-1.7099	-1.2465
2.0	-0.82270	-1.9906	0.02379	-0.61131	-0.92843	-0.7471

Table 3.16. Dimensionless Parameters for B_* Matrix Components (3rd Order Model)

$\frac{R}{L}$	b_{22*}	b_{33*}
0.01	1.44462	1.66894
0.054	1.02576	1.42373
0.1	0.92807	1.33967
0.3	0.80787]	1.18696
0.5	0.76674	1.10751
1.0	0.70339	0.98155
2.0	0.61112	0.80572

Table 3.17. Regression Parameters for Uniform Turbulence Terms

		k_1	k_2	k_3	k_4
V_z & V_x	a_*	2.0	2.894	-.1383	2.049
	b_*	2.0	3.290	+.0270	2.054
V_y	a_*	1.0	1.713	-.0790	2.048
	b_*	$\sqrt{2.0}$	2.713	+.01591	2.051

Table 3.18. Regression Parameters for Shear and Quadratic Turbulence Terms

		k_1	k_2	k_3	k_4
$V_{y,z}$ & $V_{y,x}$	a_*	.3266	1.0	.5953	-.1142
	b_*	.2811	.25	.6450	-.1500
γ_{zx}	a_*	.4343	1.0	.9170	-.1532
	b_*	.2579	.25	.6467	-.1093
$\bar{\gamma}_{zx}$ & ε_{zx}	a_*	.5342	1.0	1.276	-.2147
	b_*	.1167	.25	.7733	-.1284
$\bar{\varepsilon}_{zx}$	a_*	1.654	1.0	1.069	+2.154
	b_*	.3546	.25	.3951	+.2593
$V_{y,rr}$	a_*	1.091	1.0	.0276	+.0686
	b_*	.5508	.25	.6473	-.1365
$V_{y,rc}$ & $V_{y,rs}$	a_*	1.081	1.0	.0279	+.0685
	b_*	.3897	.25	.4567	-.0948

Table 3.19. Regression Parameters for A_* and B_* Components

	K_1	K_2	K_3	K_4
a_{21*}	0.286	-0.194	1.0	1.075
a_{22*}	1.783	-1.103	0.5	0.95
a_{31*}	0.627	-0.28	0.02	0.28
a_{32*}	1.544	-1.166	0.2	0.4
a_{33*}	1.09	-0.847	1.0	0.19
b_{22*}	0.68	-0.204	0.1	0.088
b_{23*}	1.17	-0.076	1.0	-0.28

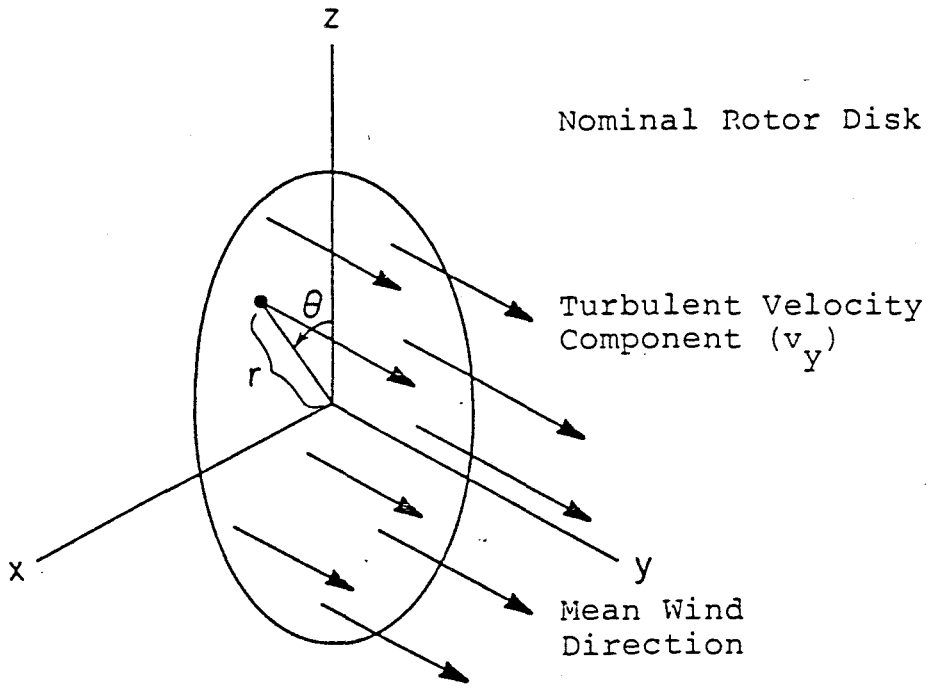

Figure 3.1. Rotor Disk Coordinates

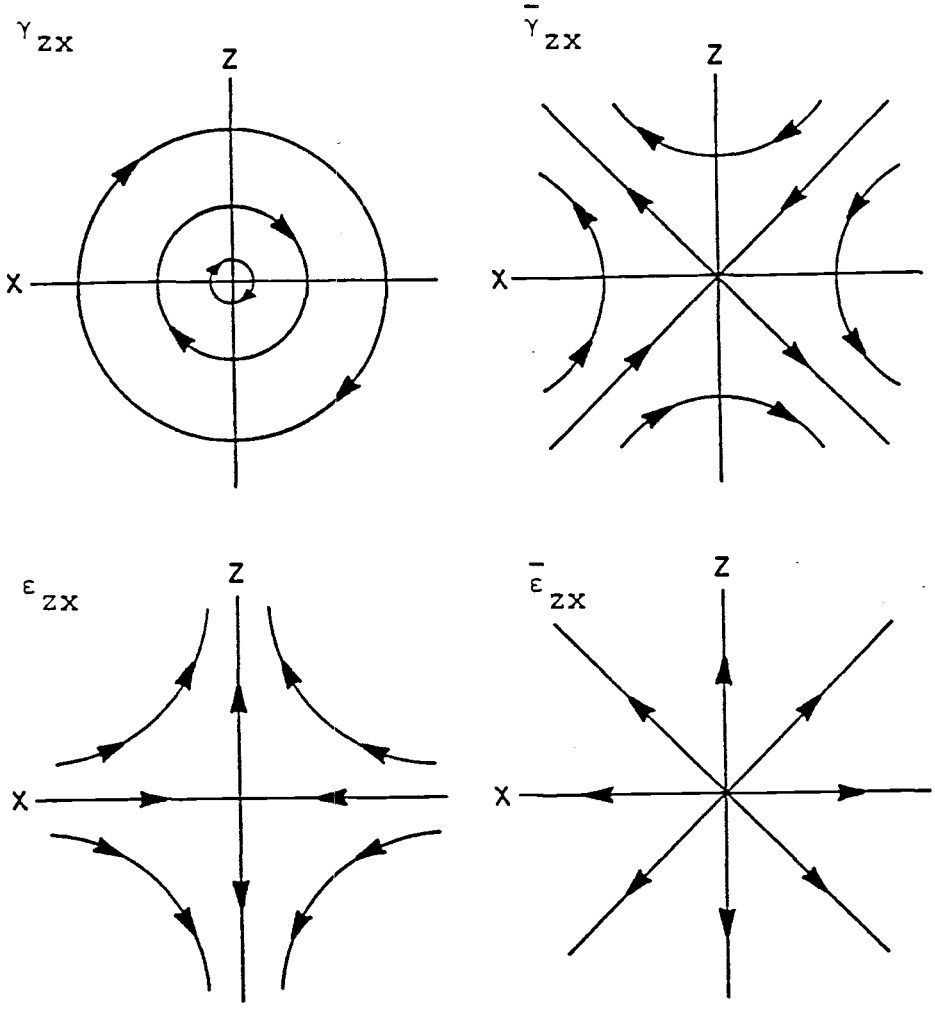

Figure 3.2. Streamlines for In-plane Velocity Gradient Terms

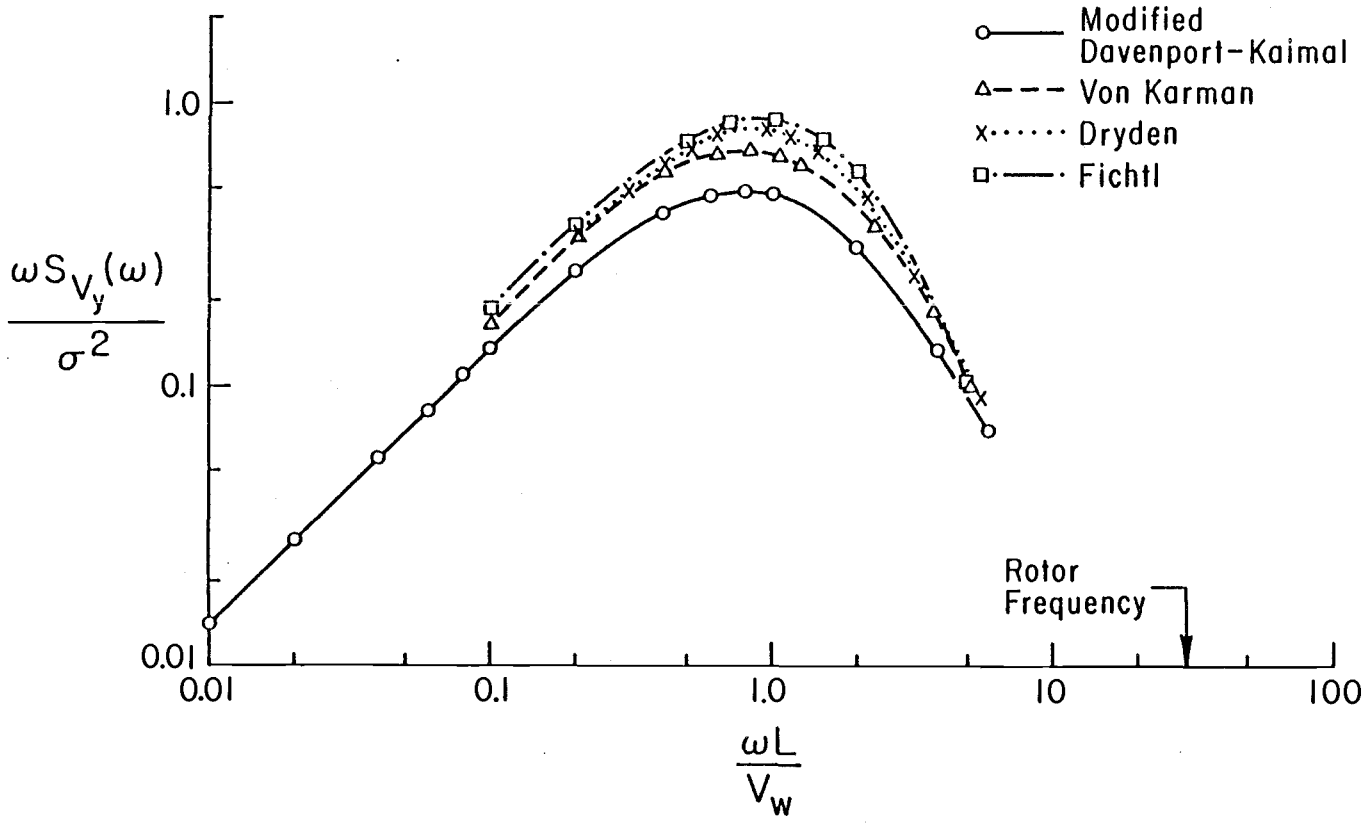

Figure 3.3. Model Comparison for Mod M, Dimensionless V_y Spectrum

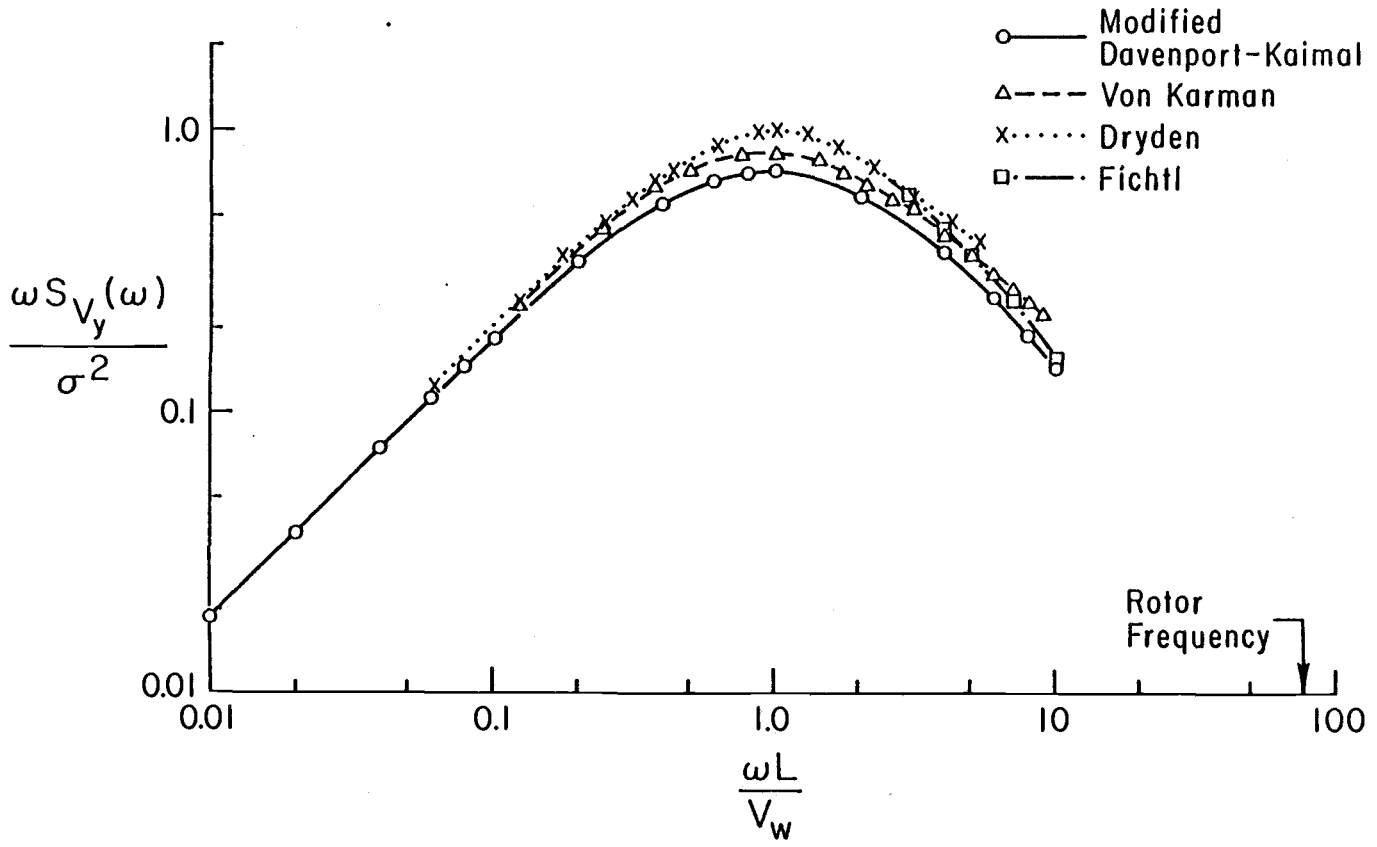

Figure 3.4. Model Comparison for Mod G, Dimensionless V_y Spectrum

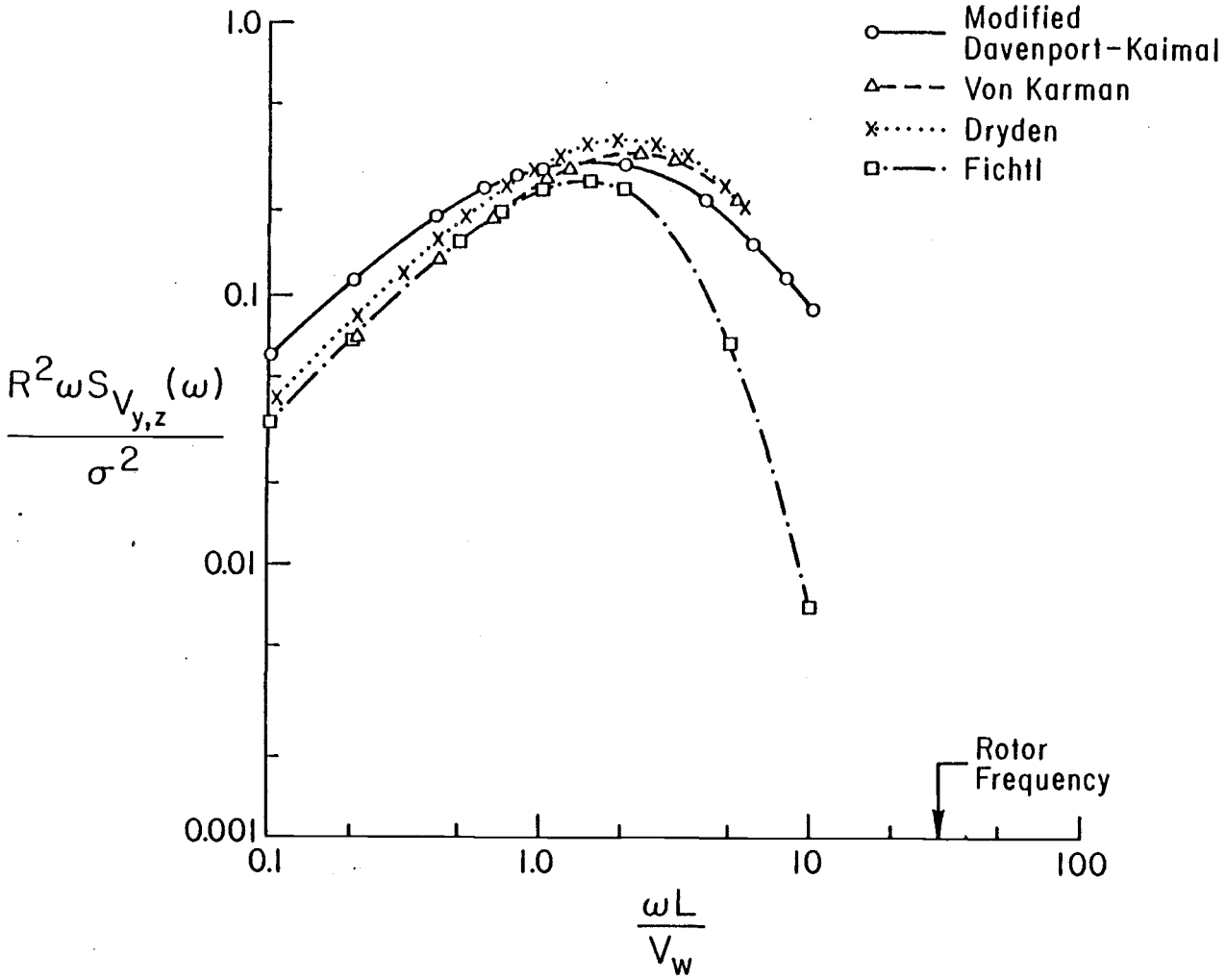

Figure 3.5. Model Comparison for Mod M, Dimensionless $V_{y,z}$ Spectrum

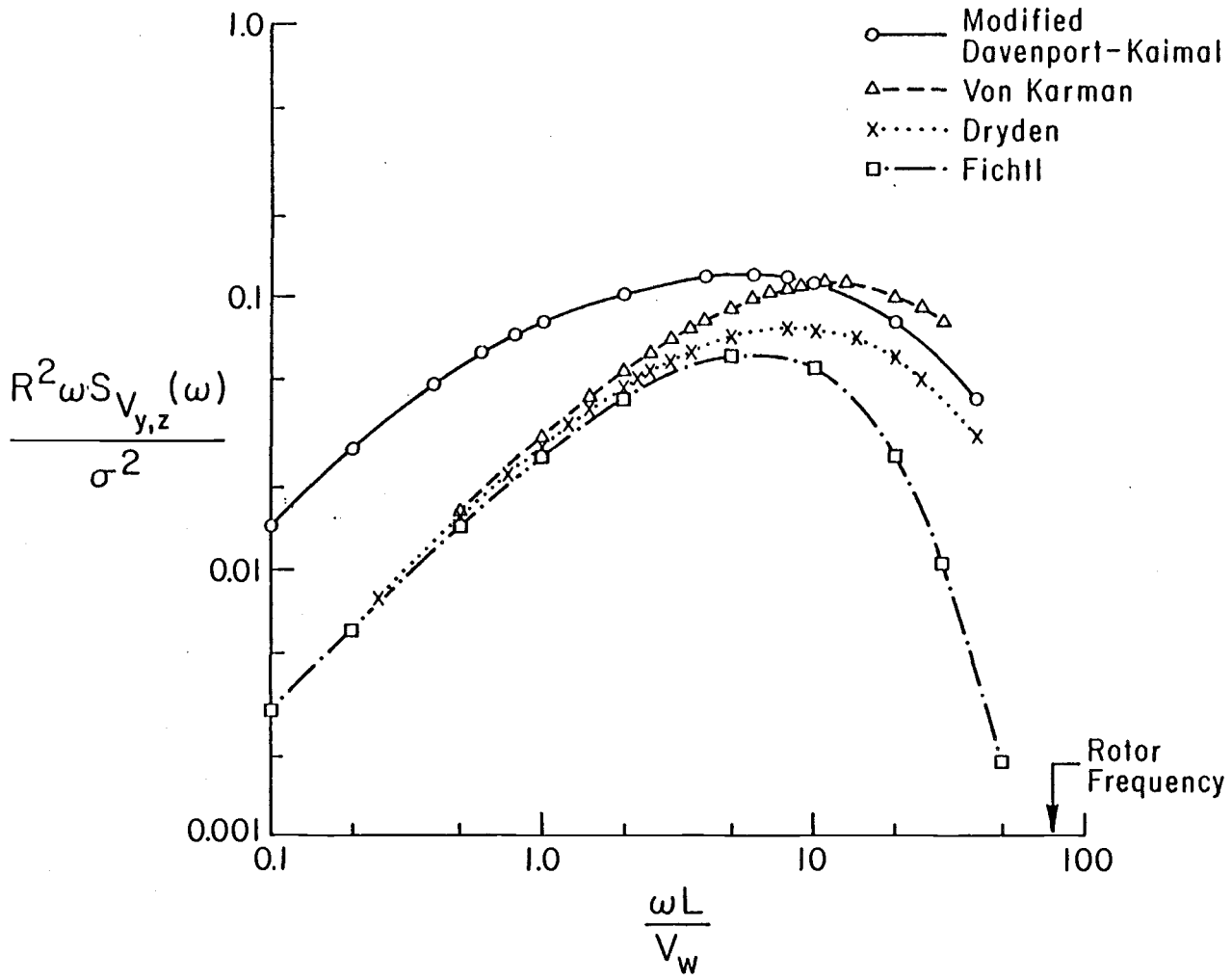

Figure 3.6. Model Comparison for Mod G, Dimensionless $V_{y,z}$ Spectrum

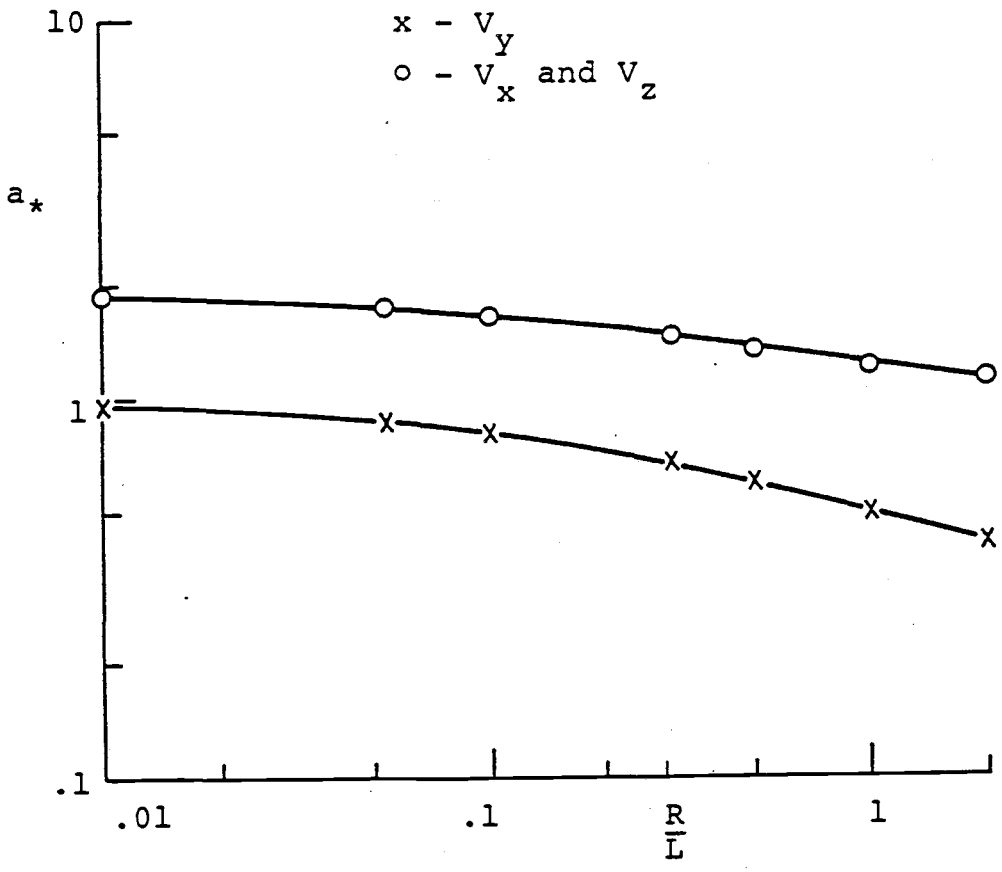

Figure 3.7. Dimensionless Parameter a_* for Uniform Turbulence Terms

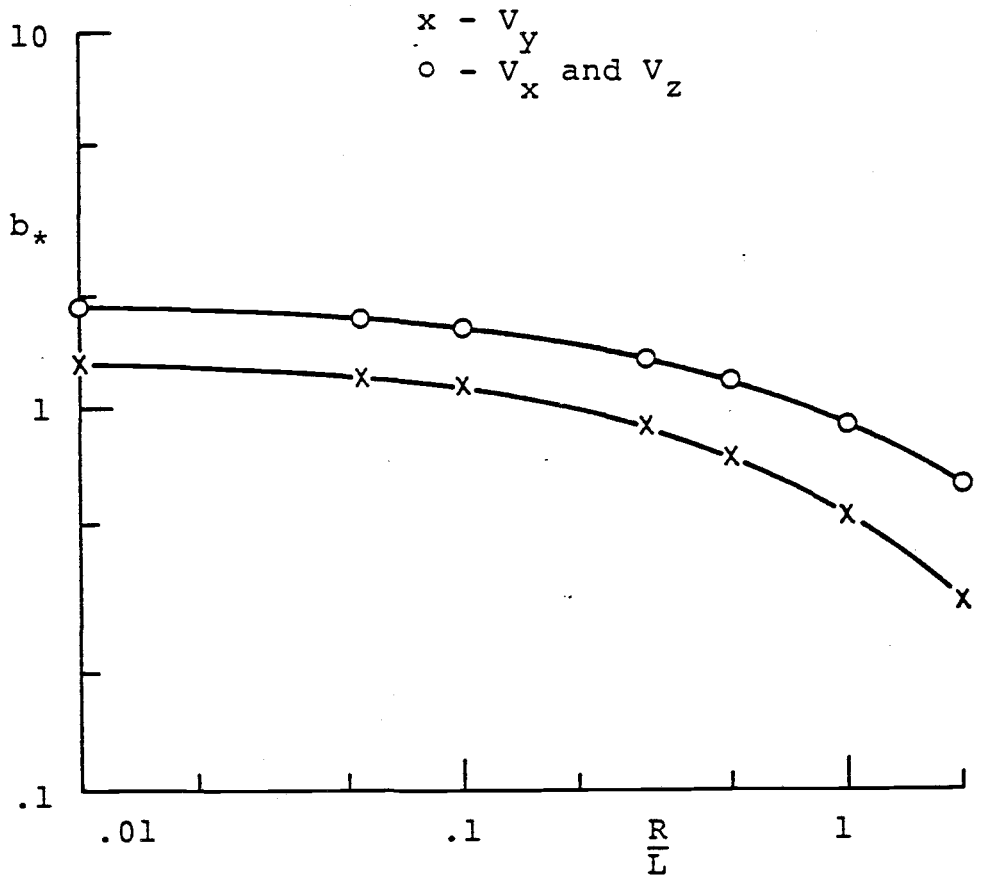

Figure 3.8. Dimensionless Parameter b_* for Uniform Turbulence Terms

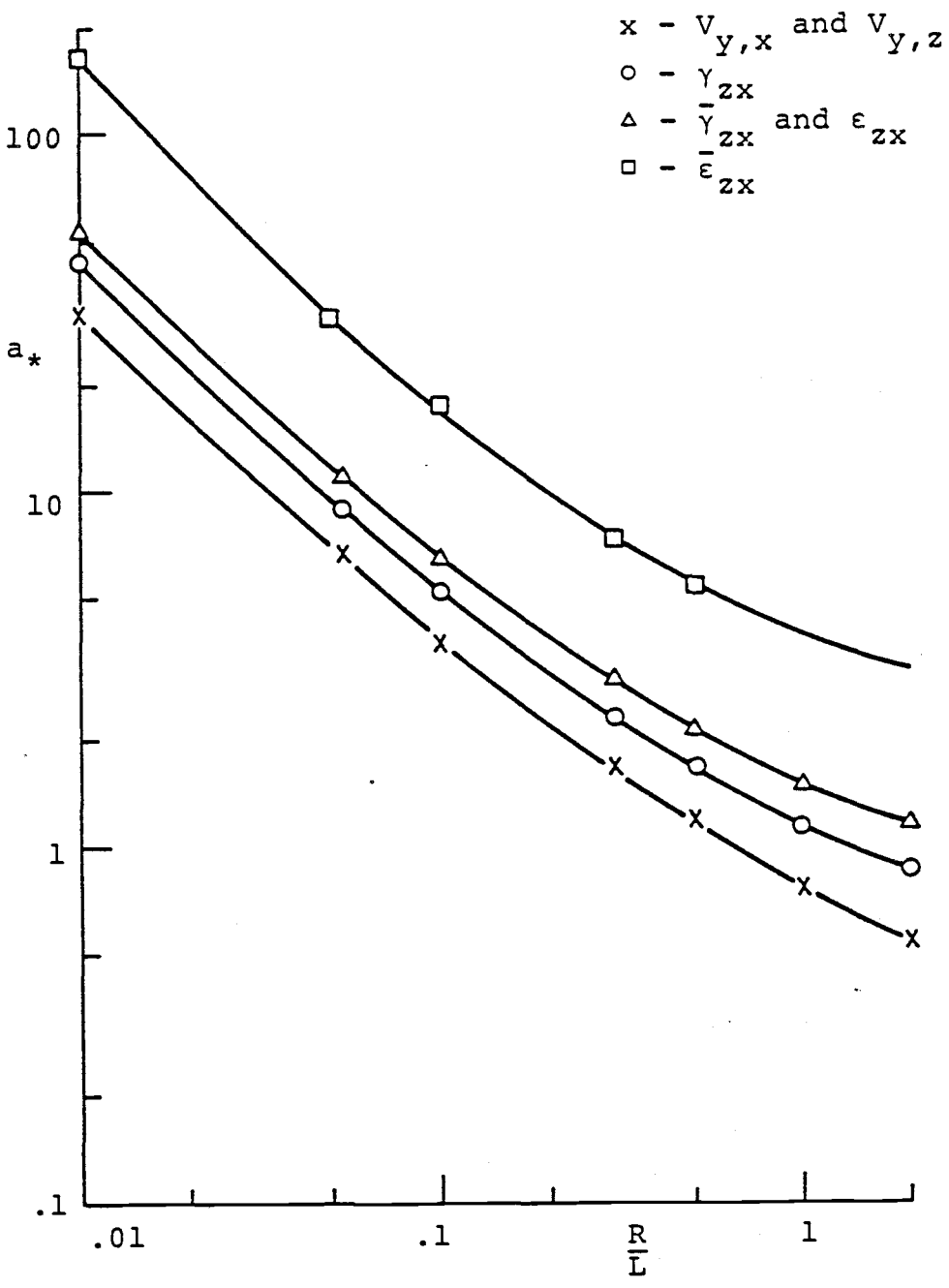

Figure 3.9. Dimensionless Parameter a_* for Gradient Turbulence Terms

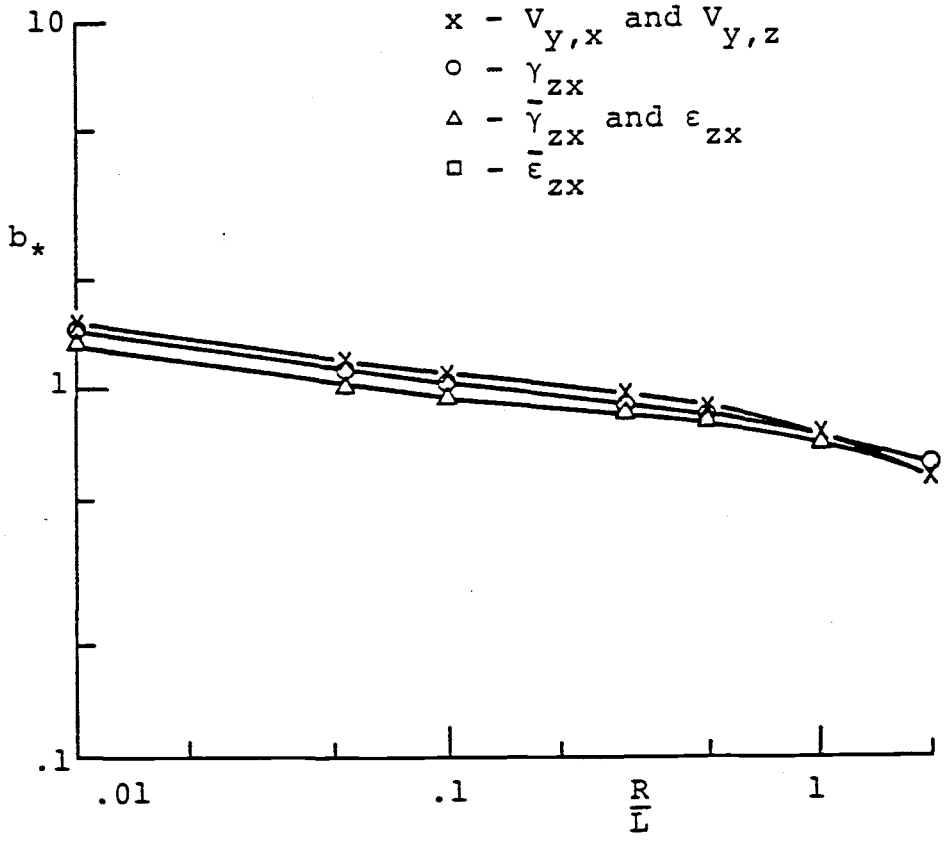

Figure 3.10. Dimensionless Parameter b_* for Gradient Turbulence Terms

IV. EVALUATION OF THE MODELING ERROR

IV.1 Introduction

Two filtered noise models for the turbulence have been presented in the previous chapter. The first model assumes all of the twelve turbulence terms are mutually uncorrelated which simplifies the model considerably. The matrices A and B in the system equation (Eq. 3.30) are diagonal. The second model assumes a third order model for V_y, $\bar{\varepsilon}_{zx}$, and $V_{y,rr}$, since these three turbulence terms are correlated due to the constraints imposed by the continuity equation. The accuracy of these filtered noise models is shown by comparison with the Von Karman model with both power spectral and correlation functions. Realistic evaluation of the modeling error can also be accomplished by comparison with experimental data using a Kalman filter and smoother.

IV.2 Model Comparison with the Von Karman Model

The filtered white noise model is often cast into the form of a stochastic differential equation

$$\dot{x} + ax = bw \tag{4.1}$$

where x = random process

w = white noise with flat PSD = S_w

The autocorrelation function and power spectrum for this process are

$$R_x(\tau) = \frac{b^2 S_w}{2a} e^{-a|\tau|} \tag{4.2}$$

$$S_x(\omega) = \frac{b^2 S_w}{a^2 + \omega^2} \tag{4.3}$$

Since the matrix A is not diagonal for the third order correlated model, we always can find a matrix which is diagonal or in Jordan canonical form by a similarity transformation (36). That is

$$A^* = Q^{-1} A Q \tag{4.4a}$$

or

$$A = Q A^* Q^{-1} \tag{4.4b}$$

where Q is the model matrix and the elements of the diagonal matrix A^* are the eigen values of the matrix A. The third order correlated model is thus decoupled into twelve stochastic differential equations of the form Eq. (4.1).

The accuracy of the approximate models given by parameters, a_* and b_* in Section III.4 depends on how accurately the autocorrelation function (Eq. 4.2) and the spectral form (Eq. 4.3) approximate the autocorrelation function and the spectra computed by integration of Eqs. (3.15) and (3.17) respectively using the Von Karman model.

For the uncorrelated model Figures 4.1 and 4.2 show the comparison for the spectrum for the uniform V_y turbulence term, and gradient $V_{y,x}$ turbulence term for R/L = 0.3. Figures 4.3 to 4.10 show the comparison of the autocorrelation function for all of the twelve turbulence components for R/L = 0.01 and 0.3. The curves show Eqs. (4.2)

and (4.3) with parameters taken from Tables 3.3 to 3.10. It can be seen from figures that the computed spectra and autocorrelation functions are reasonably well approximated by the analytical curves.

For the correlated third order model Figures 4.3, 4.8, and 4.9 show the comparison of the autocorrelation function for V_y, $\overline{\epsilon}_{zx}$, and $V_{y,rr}$ for R/L = 0.01 and 0.3. Observing the results from the figures, the correlated third order model gave a much better approximation than the uncorrelated model when compared with the Von Karman model.

IV.3 Model Verification using Real Field Data

There are essentially two approaches to verifying the turbulence input models using experimental data. In the first, since the turbulent v_y term generally provides the most important aerodynamic effect on a wind turbine, the power spectral density function predicted for v_y using the first order model, the third order model, and Von Karman model is compared with the measured spectra. In the second approach, a Kalman Filter and Smoother will be implemented using the dynamic system equations. The model outputs are then compared with the experimental data.

Before doing model verification the first step was to estimate the three turbulence parameters: namely σ, L, and V_w, which are appropriate for the site at the time the data was taken. The experimental data was obtained from the Battelle, Pacific Northwest Laboratory. An array of several anemometers was placed in fixed locations in a vertical plane (37). The anemometers were placed at eight equally spaced positions around the outer ring (Figure 4.11). One

anemometer was placed at the center of the circle. The size of the array relative to some existing large wind turbines is also included for comparison. The method used in this paper is to compute the windspeed power spectral density from the time series data. Appendix D outlines the procedures for calculation of the power spectral density. In the inertial subrange, the spectrum predicted by the Von Karman model is given approximately by

$$S(\omega) = \frac{2\sigma^2}{a^{5/3}}\left(\frac{L}{V_w}\right)^{-\frac{2}{3}} \omega^{-5/3} \qquad (4.5)$$

where $a \approx 1.339$.

Thus, using a least squares fit to spectral data over a selected bandwidth in the intertial subrange, the pareameters in Eq. (4.5) can be determined. Since the parameters V_w and σ can be estimated directly by time averaging the data, the parameter L is thus determined. Figure 4.12 shows windspeed spectral estimates at point #12. Fitting the data over the bandwidth shown in the figure gives the following parameter estimates:

$$V_w = 11.5 \text{ m/s}$$

$$\sigma = 1.6 \text{ m/s}$$

$$L = 76.5 \text{ m}$$

Also shown in Figure 4.12 is the Von Karman spectral curve from Eq. (2.4) using the above estimated parameters.

IV.3.1 Computed and Measured Spectra

Suppose we have two propeller type anemometers set up in a fixed location to measure orthogonal horizontal components of the

wind. Let $v_1(i)$ and $v_2(i)$ be sequences of measurements taken from the anemometers. If we subtract mean values from $v_1(i)$ and $v_2(i)$. The lateral and longitudinal turbulence components are thus determined from (38)

$$v_x(i) = v_2(i) \cos\phi - v(i) \sin\phi$$

$$v_y(i) = v_1(i) \cos\phi + v_2(i) \sin\phi \qquad (4.6)$$

where

$$\phi = \tan^{-1} \frac{\langle v_2 \rangle}{\langle v_1 \rangle}$$

and

$$\langle v_1 \rangle = \frac{1}{N} \sum_{i=1}^{N} v_1(i)$$

$$\langle v_2 \rangle = \frac{1}{N} \sum_{i=1}^{N} v_2(i)$$

Consider a system equation of the general form

$$\dot{x} = Ax + Bw \qquad (4.7)$$

$$y = Cx \qquad (4.8)$$

where x is the vector of system states

w is the vector of independent white noise excitations with flat PSD = Sw

y is the vector of system outputs

A, B, C are matrices.

Taking the Laplace transform of the system equation, we obtain

$$s\bar{X}(s) - x(0) = A\bar{X}(s) + B\bar{W}(s)$$

$$\bar{Y}(s) = C\bar{X}(s) \tag{4.9}$$

where the bar over a state variable denotes the Laplace transform of the same variable, for example,

$$\bar{X}(s) = \int_0^\infty x(t)e^{-st}\,dt$$

From Eqs. (4.9), we have

$$\bar{X} = (sI-A)^{-1}x(0) + (sI-A)^{-1}B\bar{W}(s) \tag{4.10}$$

$$\bar{Y} = C(sI-A)\,x(0) + C(sI-A)^{-1}B\bar{W}(s) \tag{4.11}$$

If the initial state x(0) is zero, that is, the system is relaxed at t = 0, then Eq. (4.11) reduces to

$$\bar{Y} = C(sI-A)^{-1}B\bar{W}(s)$$

$$= T(s)\bar{W}(s) \tag{4.12}$$

where $T(s) = C(sI-A)^{-1}B$ is called the transfer function matrix of the system equation. Determining the frequency response function as the transfer function evaluated for imaginary argument, i.e., $H(\omega) = T(i\omega)$, then the power spectral density of the output is

$$S_y(\omega) = H(\omega)\,H^T(-\omega)S_w \tag{4.13}$$

where $S_w = \dfrac{\sigma^2 L}{V_w^3}$

Given a sequence of measurements $v_1(i)$ and $v_2(i)$, then $y(i) = [v_1(i), v_2(i)]^T$. Eq. (4.6) can be rewritten in the matrix form

$$\begin{Bmatrix} v_1 \\ v_2 \end{Bmatrix} = \begin{bmatrix} \cos\phi & -\sin\phi \\ \sin\phi & \cos\phi \end{bmatrix} \begin{Bmatrix} v_y \\ v_x \end{Bmatrix} \tag{4.14}$$

Substituting Eqs. (3.8) and (3.13) for v_y and v_x the measurement matrix C can thus be determined.

To determine how accurate the model is, we can calculate the power spectral density predicted by the model in the case when $\phi = 0$ for the first order model, the third order model, and the Von Karman model and compare with the power spectral density of the measurement from the experimental data. From Figure 4.21 the PSD for v_y predicted by the first order model and the third order model compares very well with the PSD from Von Karman model and experimental data. It is, at first, surprising that the third order model does not approximate the Von Karman model more closely. This result can be explained by the fact that both approximate models neglect the small turbulence eddies which vary considerably over the rotor disk. Thus it is expected that single point measurements and the Von Karman model would show more high frequency energy than predicted by the approximate models. The approximate model should do a better job when averages over several points on the rotor disk are considered.

IV.3.2 Kalman Filter and Smoother

Before presenting the Kalman Filter and Smoother for system verification first the relationship between the discrete time and continuous time system will be discussed. Consider a continuous system equation of the form

$$\dot{x}(t) = Ax(t) + Bw(t), \quad x(0) = x_0 \tag{4.15}$$

where A is nxn matrix

B is nxp matrix

x is the vector of system state

w is the vector of independent white noise excitations.

The solution (39) of Eq.(4.15) for a given w(t) is

$$x(t) = \phi(t)x_0 + \int_0^t \phi(t-\tau)Bw(\tau)\, d\tau \tag{4.16}$$

where ϕ is the state transition matrix of $\dot{x} = Ax$: or correspondingly, the unique solution of

$$\dot{\phi}(t) = A\phi(t), \quad \phi(0) = I \tag{4.17}$$

and $\phi(t) = e^{At}$

Using Eq. (4.16) the sampled state satisfies the difference equation

$$x(k+1) = \phi\, x(k) + \xi(k) \tag{4.18}$$

where Δ = Sampling period

$$\xi(k) = \int_0^{\Delta} \phi(\Delta-\tau)Bw(t_k+\tau)d\tau. \tag{4.19}$$

It is shown in Appendix E that the sequence $\xi(k)$ is a normally distributed and sequentially uncorrelated random sequence and can be represented by

$$\xi(k) = \Gamma u(k) \tag{4.20}$$

where each component of u(k) is normal with zero mean and unit variance and mutually uncorrelated.

Thus, the state equation is given by

$$x(k+1) = \phi x(k) + \Gamma u(k) \tag{4.21}$$

where x(k) is the state vector, having dimension n

ϕ is a known nxn state t ansition matrix

Γ is a known nxp matrix

u(k) is normally distributed, sequentially uncorrelated process noise with zero mean and covariance Q, having dimension p.

The output is sampled at discrete time, that is

$$y(k) = Cx(k) + v(k) \tag{4.22}$$

where y(k) is observation vector with dimension m

v(k) is normally distributed, sequentially uncorrelated measurement noise with zero mean and covariance R, having dimension m

C is mxn observation matrix.

The filtering problem is a sequential, weighted least squares problem in which information about x is lost (due to u(k)) as the process evolves from stage k to k+1, and new information is added in stage k+1 when y(k+1) is available (40). The complete transition solution to the filtering problem was given by Kalman (41). The Kalman solution is stated in a computationally convenient form in which the best estimate $\hat{x}(k)$, and the error covariance matrix P(k), are propagated from stage to stage. This solution is summarized in Eqs. (4.23) through (4.27)

Covariance Filter

Time update

$$\hat{x}(k+1) = \phi\hat{x}(k+) \tag{4.23}$$

$$P(k+1) = \phi P(k+)\phi^T + \Gamma Q\Gamma^T \tag{4.24}$$

Measurement Update

$$\hat{x}(k+) = \hat{x}(k) + K(k)(y(k) - C\hat{x}(k)) \tag{4.25}$$

$$P(k+) = P(k) - K(k)CP(k) \tag{4.26}$$

$$K(k) = P(k)C^T (CP(k)C^T + R)^{-1} \tag{4.27}$$

The notation $\hat{x}(k+)$ and $P(k+)$ indicate the state estimate and covariance at stage k after incorporating the measurement, y(k).

The conventional filter may also be implemented (42) in a form which propagates the information matrix Y.

Information Filter

Time Update

$$d(k+1) = \phi^{-T} d(k+) - L(k)\Gamma\phi^{-T}d(k+) \tag{4.28}$$

$$Y(k+1) = E(k) - L(k)\Gamma^T E(k) \tag{4.29}$$

$$E(k) = \phi^{-T} Y(k+) \phi^{-1} \tag{4.30}$$

$$L(k) = E(k) \Gamma (\Gamma^T E(k)\Gamma + Q^{-1})^{-1} \tag{4.31}$$

Measurement Update

$$d(k+) = d(k) + C^T R^{-1} y(k) \tag{4.32}$$

$$Y(k+) = Y(k) + C^T R^{-1} C \tag{4.33}$$

The information matrix Y(k) is defined as $P^{-1}(k)$ and $\hat{x}(k)$ is related to d(k) by

$$d(k) = Y(k)\hat{x}(k) \tag{4.34}$$

$$d(k+) = Y(k+)\hat{x}(k+) \tag{4.35}$$

Note that the information filter simply propagates the information matrix from stage to stage, accounting for the loss of information in a time update, and gain of information in a measurement update.

The covariance filter is the more popular form as it yields $\hat{x}(k)$ directly, and is more efficient than the information filter when $m < p$, as is often the case. However, the information filter can be applied successfully when either poor or no a priori information leads to starting difficulties in the covariance implementation. There is no problem initializing the information filter in the absence of a priori information, as Y(o) and d(o) are set to zero, and Y(k) and d(k) are propagated from measurement to measurement until Y(k) can be inverted to find $\hat{x}(k)$. Here, the information filter will be implemented in this research for system verification.

Use of the usual Kalman Filter equations for calculation of the error covariance can result in a matrix which fails to be non-negative definite. This may occur particularly if at least some of the measurements are very accurate, since numerical computation using ill-conditioned quantities is involved. As a technique for coping with this difficulty, Potter (43) suggested that the error covariance matrix be propagated in square root form. His original ideas were, however, restricted to the case of zero process noise and scalar measurements. This method is completely successful in maintaining the positive semidefinite nature of the error covariance,

and it can provide twice the effective precision of the conventional filter implementation in ill-conditioned problems. Potter's ideas were later extended to cope with the presence of process noise and vector measurements (44, 45).

Let M be a nonnegative definite symmetric matrix. A square root of M is a matrix N, normally square, but not necessarily nonnegative definite symmetric, such that $M = NN^T$. The square root information matrix, W, is defined in Eqs. (4.36) and (4.37)

$$W^T(k)W(k) \triangleq Y(k) \tag{4.36}$$

$$W^T(k+)W(k+) \triangleq Y(k+) \tag{4.37}$$

Similarly, the process and measurement noise covariance square roots are defined by

$$U(k)U^T(k) = Q \tag{4.38}$$

$$V(k)V^T(k) = R \tag{4.39}$$

Square root forms of the time and measurement update procedures for the information filter (46) are summarized in Eqs. (4.40) through (4.47).

Square Root Information Filter

Time Update Implementation I

$$b(k+1) = b(k+) - L(k)b(k+) \tag{4.40}$$

$$W(k+1) = W(k+)\phi^{-1} - L(k)W(k+)\phi^{-1} \tag{4.41}$$

$$L(k) = F(k)\,(G(k) + U^{-1}(k))^{-1}G^{-T}(k)F^{T}(k) \tag{4.42}$$

$$F(k) = W(k+)\phi^{-1}\Gamma \tag{4.43}$$

$$G(k) = (F^{T}(k)F(k) + Q^{-1})^{T/2} \tag{4.44}$$

Time Update Implementation II

$$\left[\begin{array}{c|c|c} A(k+1) & B(k+1) & c(k+1) \\ \hline 0 & W(k+1) & b(k+1) \end{array}\right] = T \left[\begin{array}{c|c|c} U(k) & 0 & 0 \\ \hline W(k+)\phi^{-1}\Gamma & W(k+)\phi^{-1} & b_{k+} \end{array}\right] \tag{4.45}$$

Measurement Update

$$\left[\begin{array}{c|c} W(k+) & b(k+) \\ \hline 0 & e_k \end{array}\right] = T \left[\begin{array}{c|c} W(k) & b(k) \\ \hline V^{-1}(k)C & V^{-1}(k)y(k) \end{array}\right] \tag{4.46}$$

where $b(k) = W(k)\,\hat{x}(k)$

and A(k+1) in Eq. (4.45) and W(k+) in Eq. (4.46) are upper triangular. The appropriate T in Eq.p(4.45) and (4.46) is obtained by the triangularization algorithm given in Appendix C.

The discussions so far have been chiefly concerned with the Kalman filtering problem which seeks $\hat{x}(k)$, the best estimate of $x(k)$ given all measurements through $y(k)$. The smoothing problem seeks $\hat{x}(k/N)$, the best estimate of $x(k)$ given all measurements through $y(N)$, where N is some arbitrary index greater than or equal to k. The smoothed solution, $\hat{x}(k/N)$, minimizes the performance index (47)

$$J = ||x(0)-\hat{x}(0)||^2_{P^{-1}(0)} + \sum_{i=0}^{N-1} [||u(i)||^2_{Q^{-1}} + ||v(i+1)||^2_{R^{-1}}] \tag{4.48}$$

subject to the constraints

$$x(k+1) = \phi x(k) + \Gamma u(k); \qquad k=0, N-1 \tag{4.49}$$

$$y(k) = cx(k) + v(k); \qquad k=1,N \tag{4.50}$$

Meditch (48) has classified three types of smoothing solutions: fixed interval, fixed point, and fixed lag. Here, we focus on the fixed interval smoother. Fixed interval smoothing assumes that a total of N measurements are made, and the complete state space trajectory ($\hat{x}(k/N)$, k = 0,N) is required.

The square root information smoother (SRIS) for fixed interval smoothing was motivated by the square root information filter (SRIF). The complete smoothed solution is determined by the following computational procedures (49):

Define

$$b^{(p+1)}(k/N) \triangleq b(k+1/N) \tag{4.51}$$

$$W^{(p+1)}(k/N) \triangleq W(k+1/N) \tag{4.52}$$

$$\phi^{(i)} \triangleq \begin{cases} \phi & ; \quad i=1 \\ I & ; \quad i\neq 1 \end{cases} \tag{4.53}$$

and for i = p, 1 compute

$$\left[\begin{array}{c|c|c} A^{(i)}(k/N) & B^{(i)}(k/N) & C^{(i)}(k/N) \\ \hline 0 & W^{(i)}(k/N) & b^{(i)}(k/N) \end{array}\right] T = \left[\begin{array}{c|c|c} \Gamma^{(i)}(k)+B^{(i)}(k)\Gamma^{(i)} & B^{(i)}(k)\phi^{(i)} & C^{(i)}(k) \\ \hline W^{(i+1)}(k/N)\Gamma^{(i)} & W^{(i+1)}(k/N)\phi & b^{(i+1)}(k/N) \end{array}\right] \tag{4.54}$$

Then

$$b(k/N) \triangleq b^{(1)}(k/N) \tag{4.55}$$

$$W(k/N) \triangleq W^{(1)}(k/N) \tag{4.56}$$

$$W(k/N)\hat{x}(k/N) = b(k/N) \tag{4.57}$$

$$P(k/N) = W^{-1}(k/N)W^{-T}(k/N) \tag{4.58}$$

In Eq. (4.54), only $W^{(1)}(k/N)$ is triangularized. The complete smoothed solution is generated by processing through Eqs. (4.51) to (4.58) for k = N-1, 0.

The fixed interval smoothing solutions consist of processing the filtering algorithm (SRIF) which is a forward sweep from stage

0 to N, and a backward sweep to stage 0 using SRIS to obtain the smoothed solutions. When dealing with the model verification, a reasonable criterion is the residual of the model output. That is the difference between the output predicted by the model using the smoothed states and the experimental data. Unfortunately the residual is very small due to the accuracy of the experimental data.

Another criterion was set up as follows:

1. Using the one-step predictor to calculate the current smoothed state.
2. Calculating the residuals.

That is,

$$I(k) = y(k) - C\phi\hat{x}(k-1/N) \tag{4.59}$$

where $I(k) = [I_1(k) \quad I_2(k)]^T$.

Here the error of the criterion includes the one-step model noise error and measurement error and theoretically is a white noise process. The sequence I(k) was calculated at points #10 and #12 in terms of mean value, variance, and power spectral density (Figs. 4.14 and 4.15). In addition these results are compared to the prediction with no model which assumes $\hat{x}(k-1/N)$ is equal to zero and the error variance is just the measurement variance itself.

The results show that I(k) is white noise with mean value and variance shown on Table 4.1. The experimental data variance is also shown on Table 4.1. The first order and the third order model indeed can predicate the model output well, since the variances of the models are much smaller than the variance of the experimental data. The

results also indicate that the third order model gives a slightly better approximation to the experimental data than the first order model.

Table 4.1. The Mean Values and Variances of the Sequence I(k)

	Mean Values (m/sec)		Variance ((m/sec)^2)		
	1st order model	3rd order model	1st order model	3rd order model	no model
At #10					
	-.0019	-.0023	.08816	.08431	1.9502
	-.0023	-.0022	.1251	.1249	.9840
At #12					
	.0025	.0021	.1506	.1308	3.1784
	-.0020	-.0018	.2090	.2044	1.0236

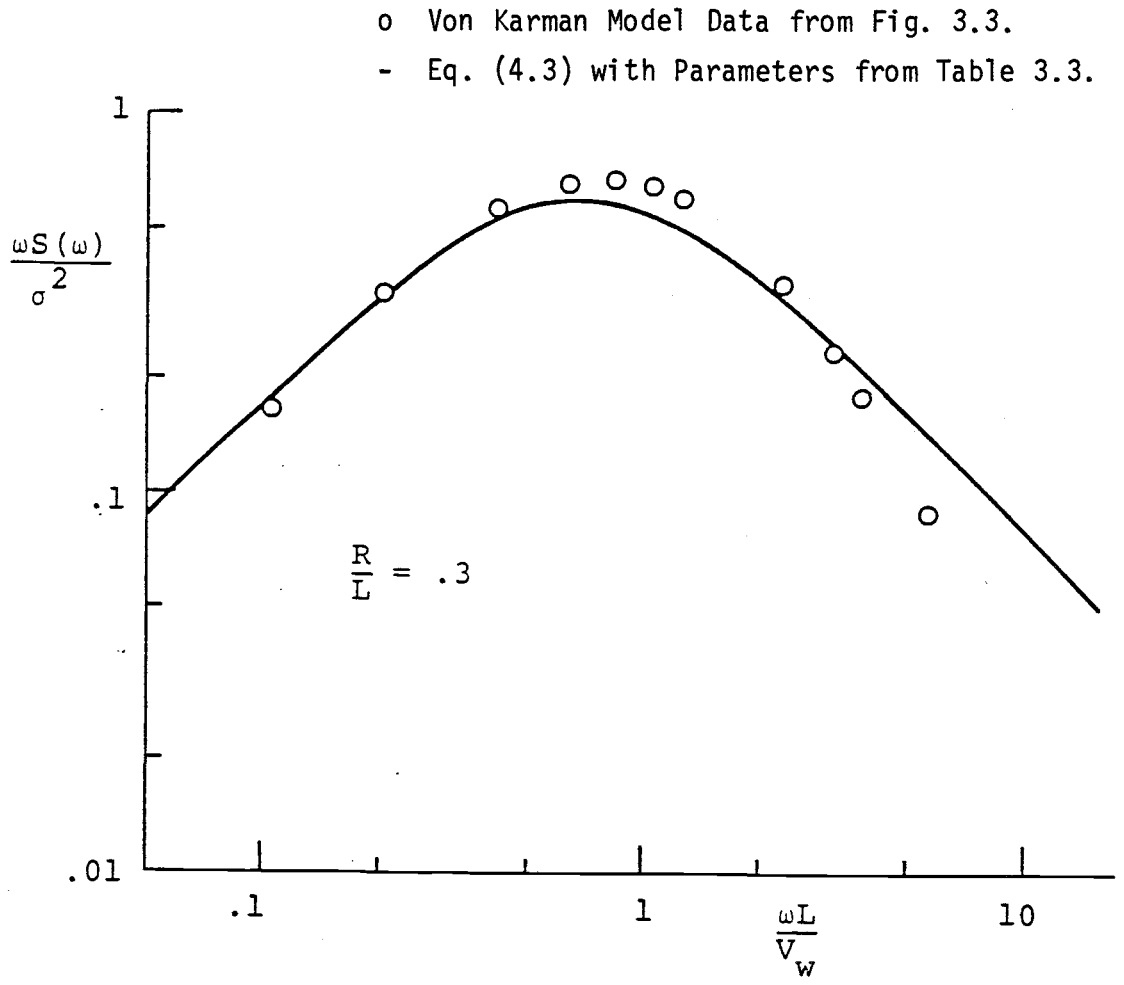

Figure 4.1. Dimensionless Spectrum for Uniform V_y Turbulence Term

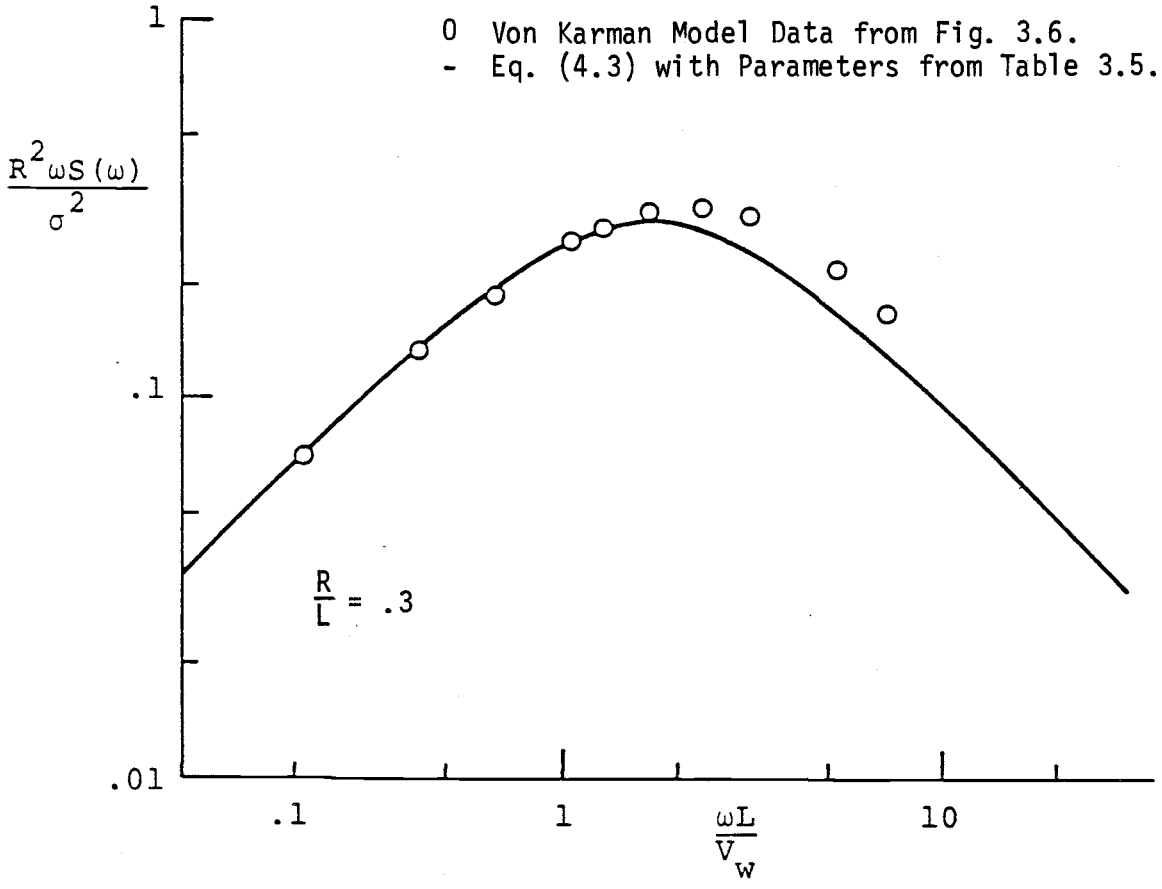

Figure 4.2. Dimensionless Spectrum for Gradient $V_{y,x}$ Turbulence Term

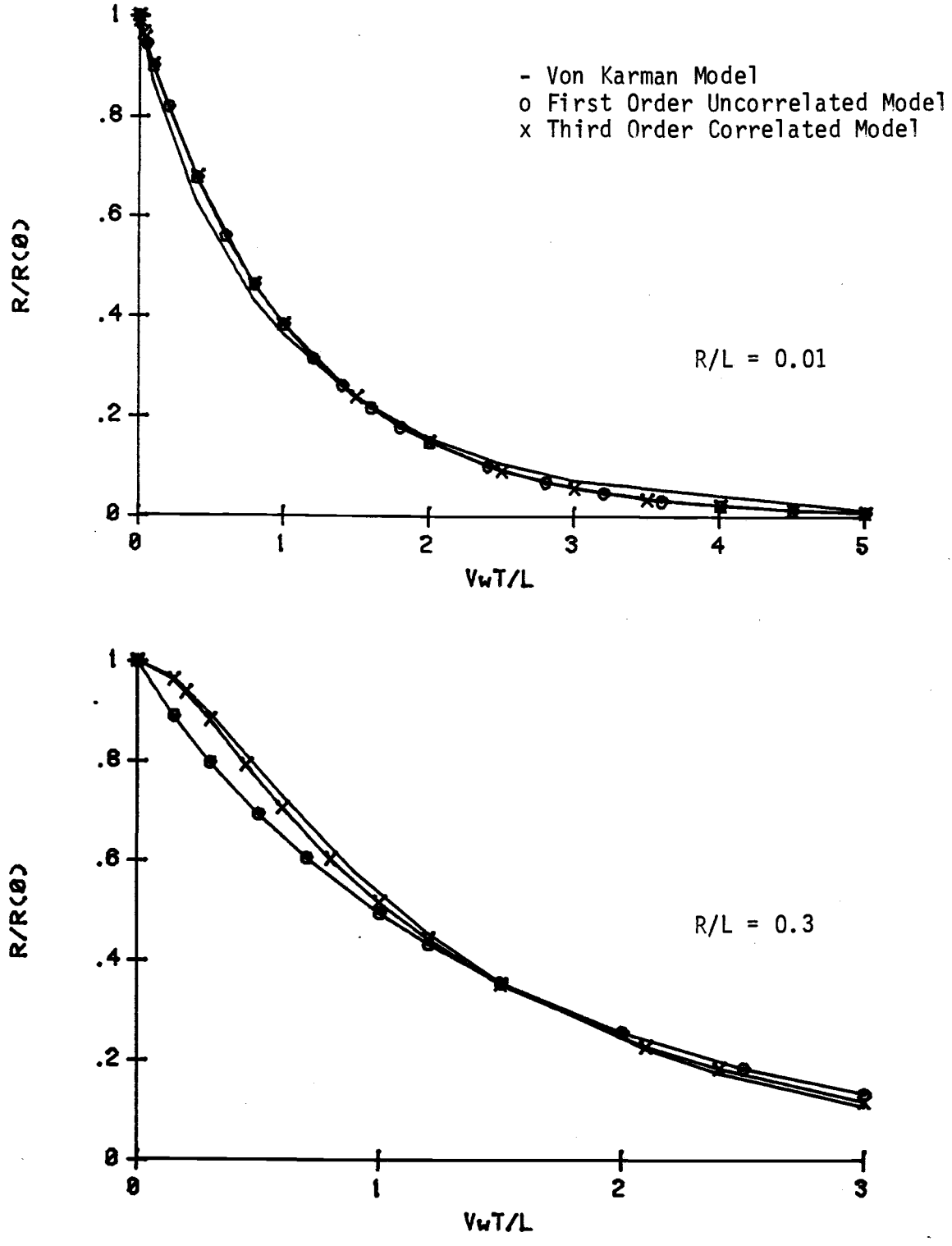

Figure 4.3. Dimensionless Autocorrelation Function for V_y Turbulence Term

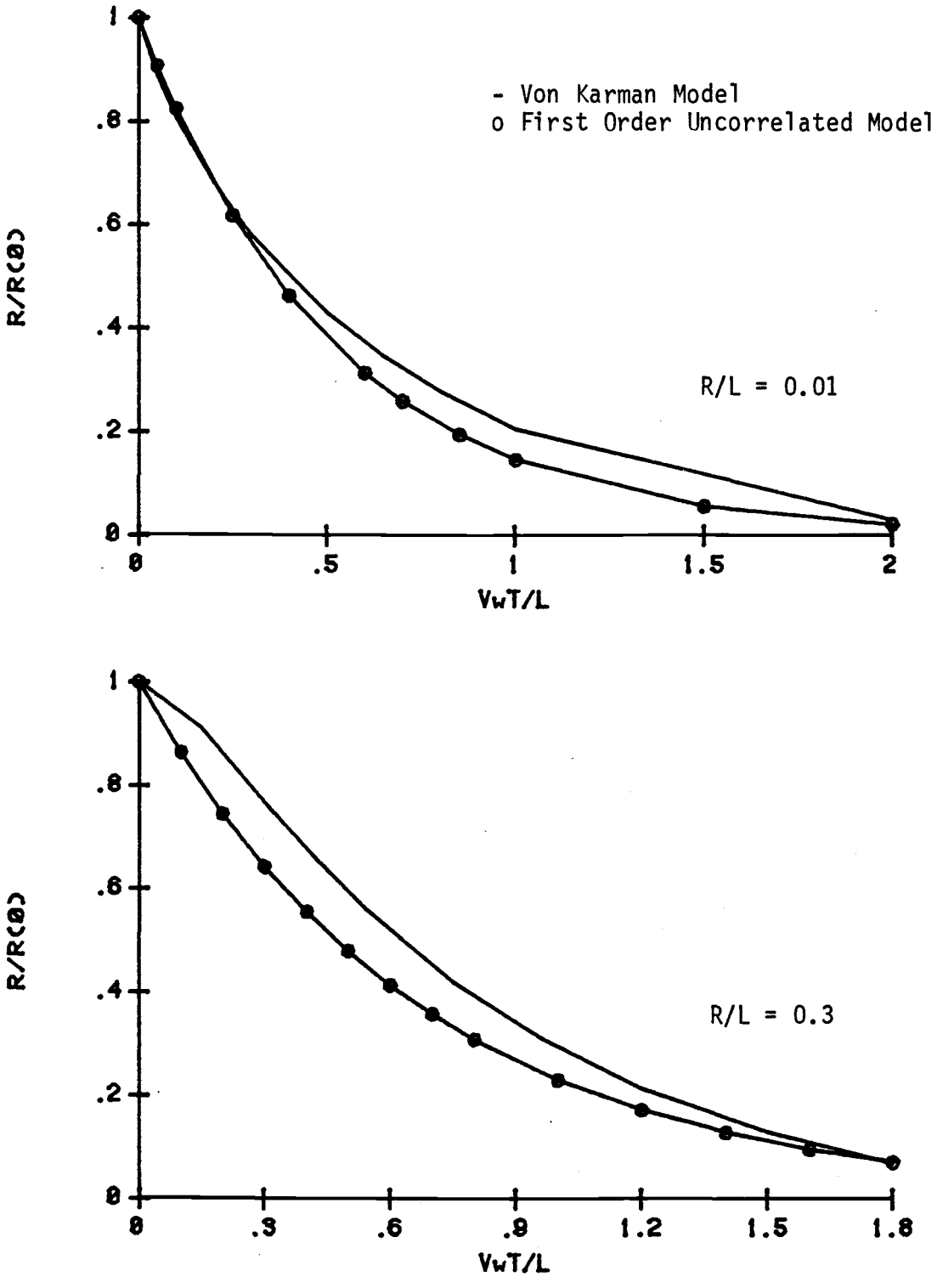

Figure 4.4. Dimensionless Autocorrelation Function for V_x & V_z Turbulence Terms

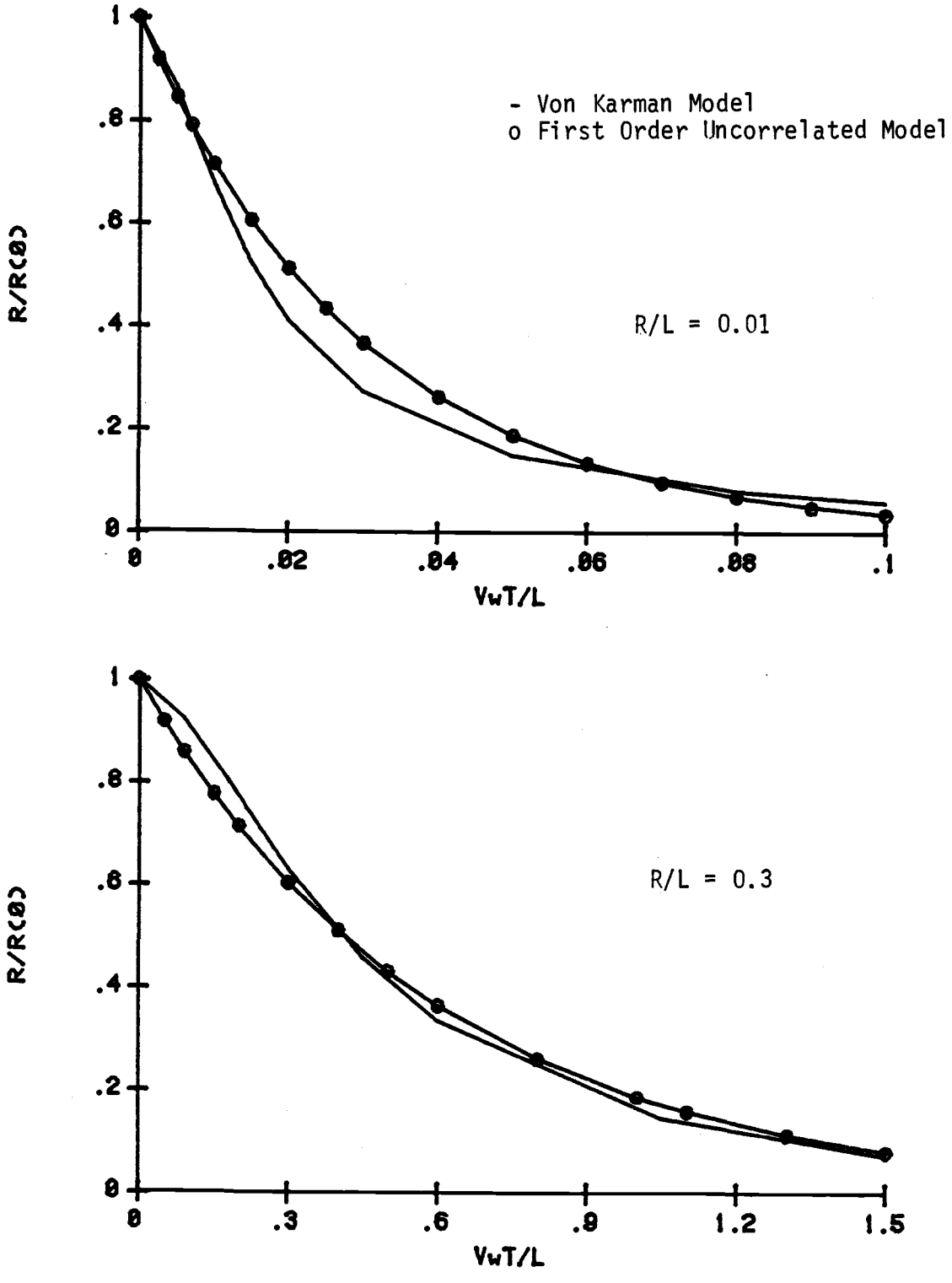

Figure 4.5. Dimensionless Autocorrelation Function for $V_{y,x}$ & $V_{y,z}$ Turbulence Terms

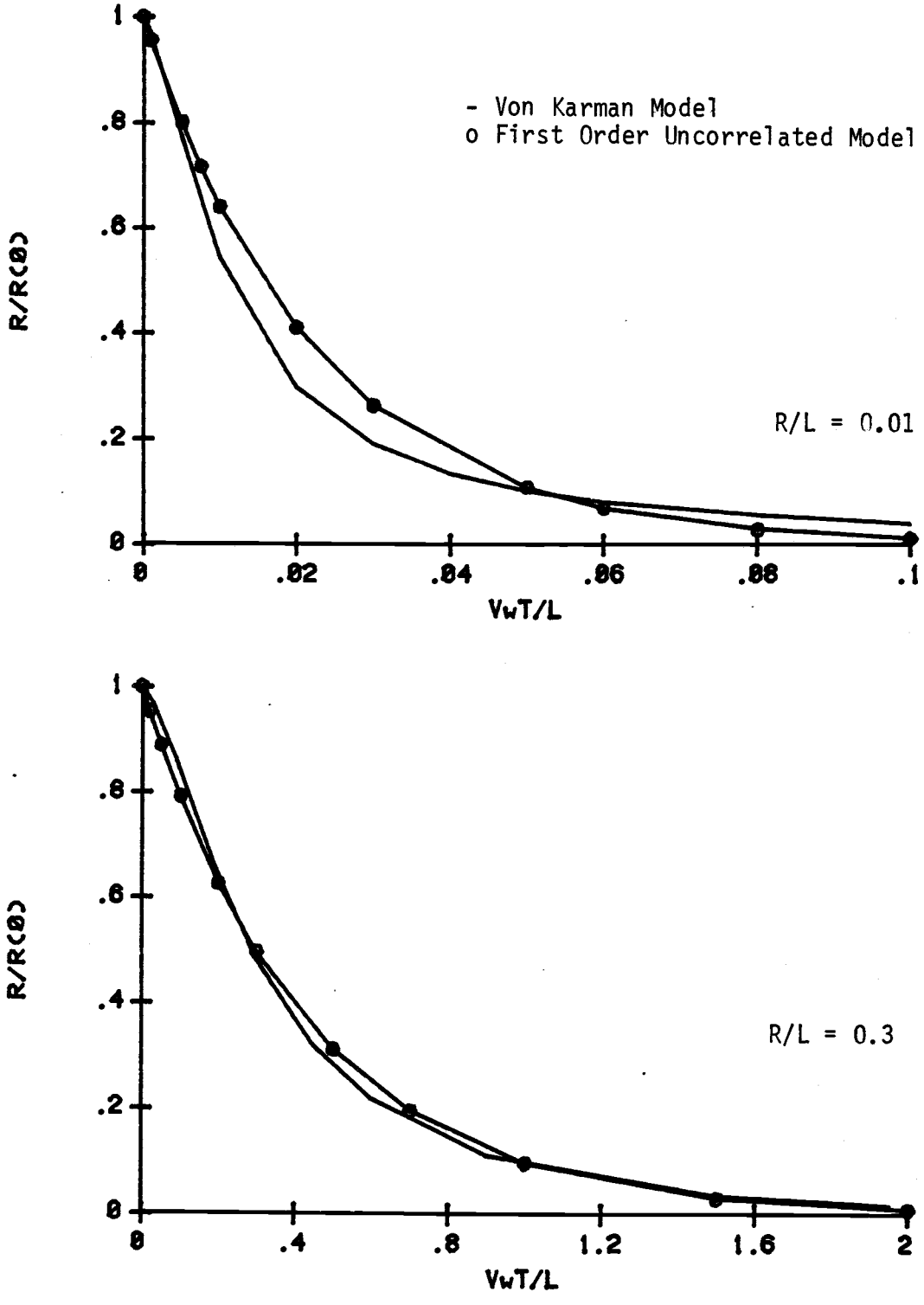

Figure 4.6. Dimensionless Autocorrelation Function for γ_{zx} Turbulence Term

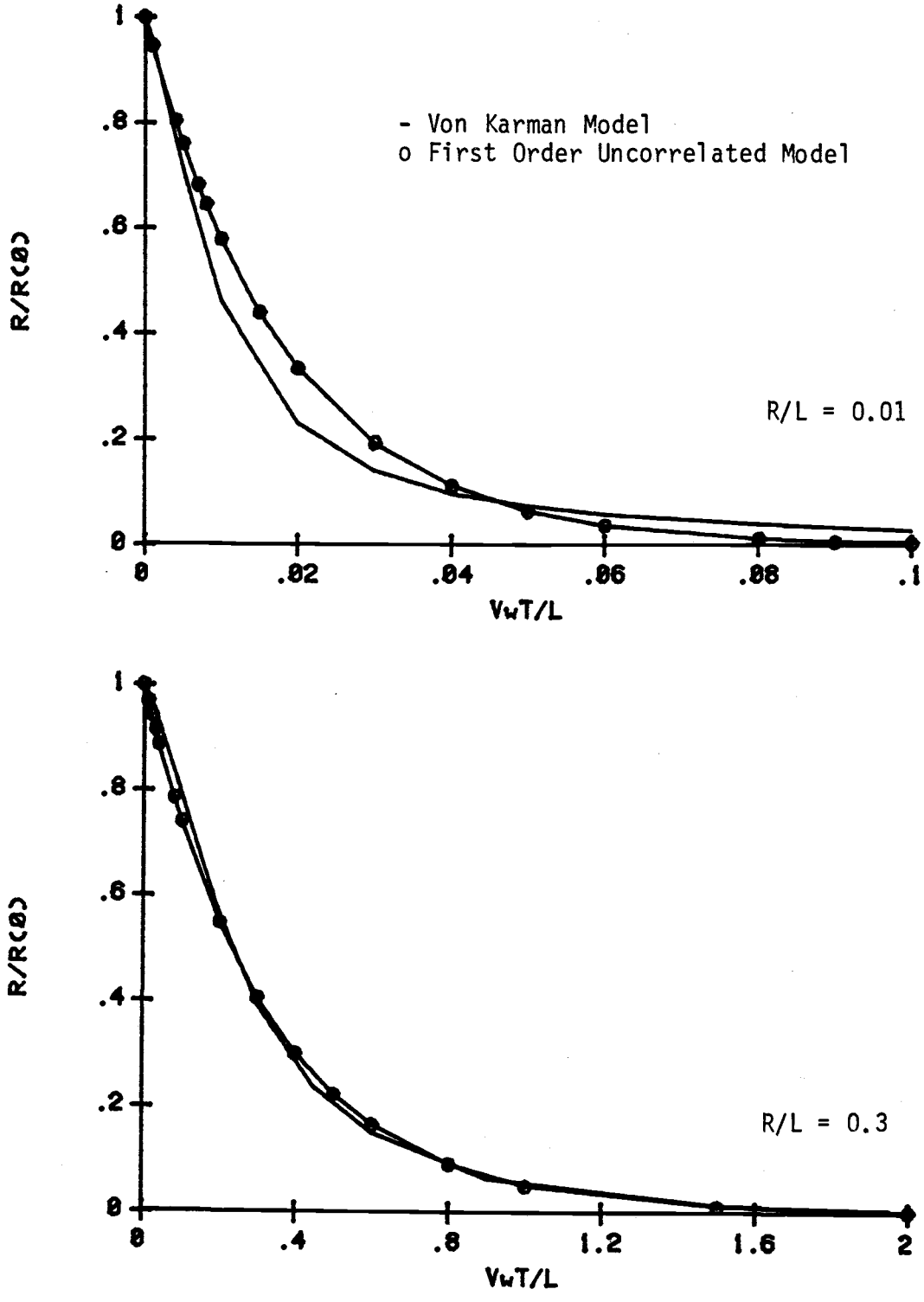

Figure 4.7. Dimensionless Autocorrelation Function for γ_{zx} & ϵ_{zx} Turbulence Terms

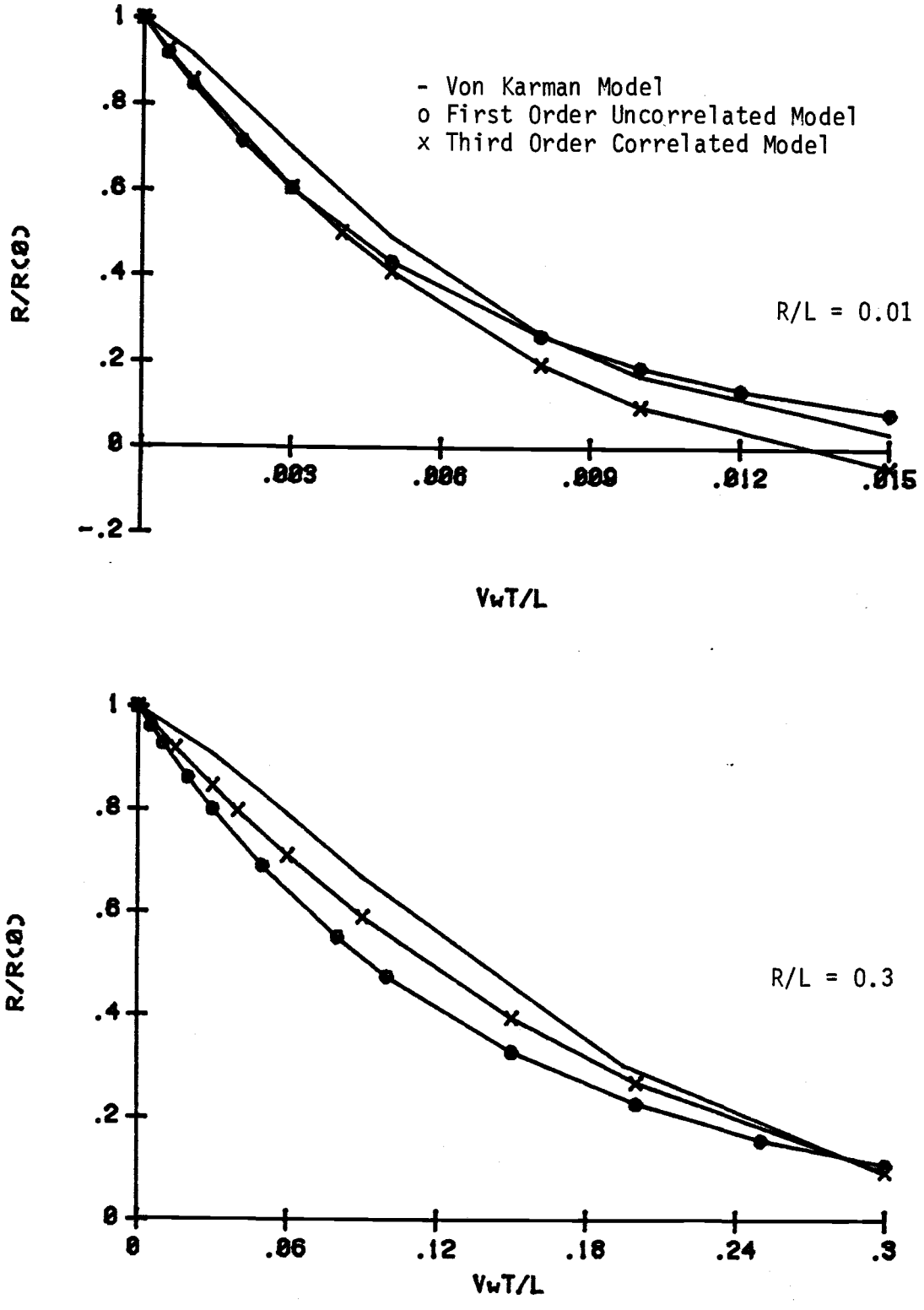

Figure 4.8. Dimensionless Autocorrelation Function for $\overline{\epsilon}_{zx}$ Turbulence Term

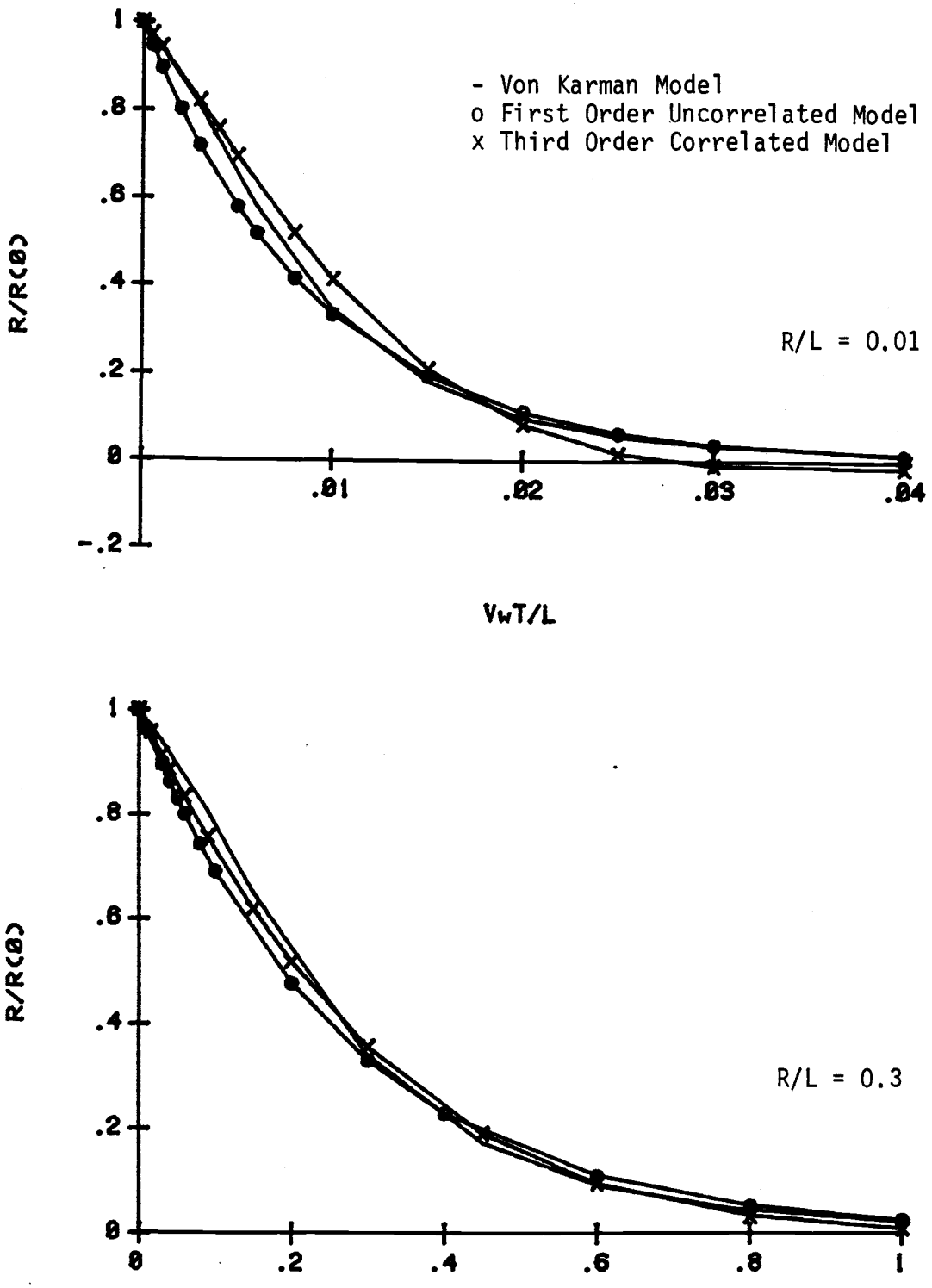

Figure 4.9. Dimensionless Autocorrelation Function for $V_{y,rr}$ Turbulence Term

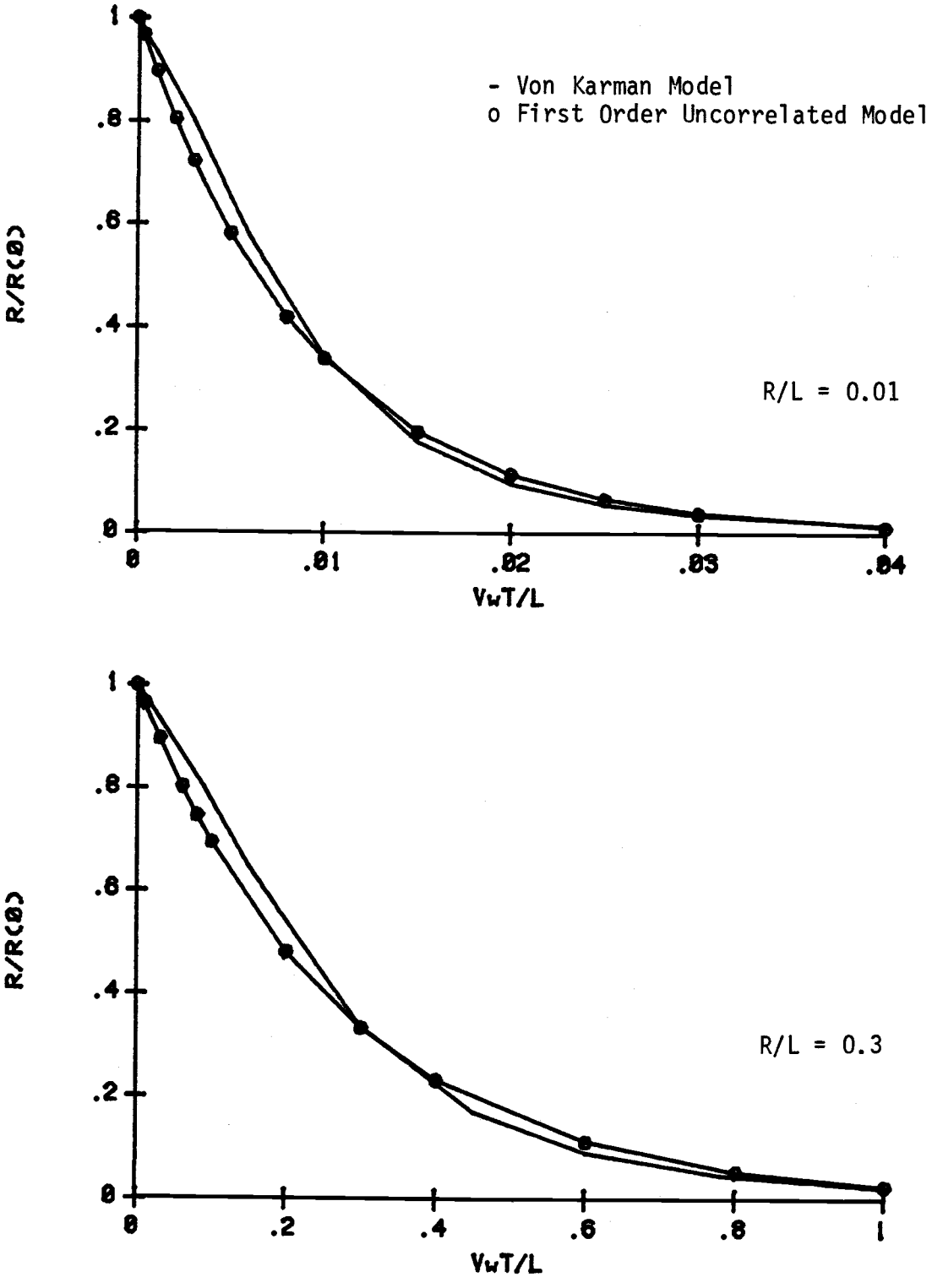

Figure 4.10. Dimensionless Autocorrelation Function for $V_{y,rc}$ & $V_{y,rs}$ Turbulence Terms

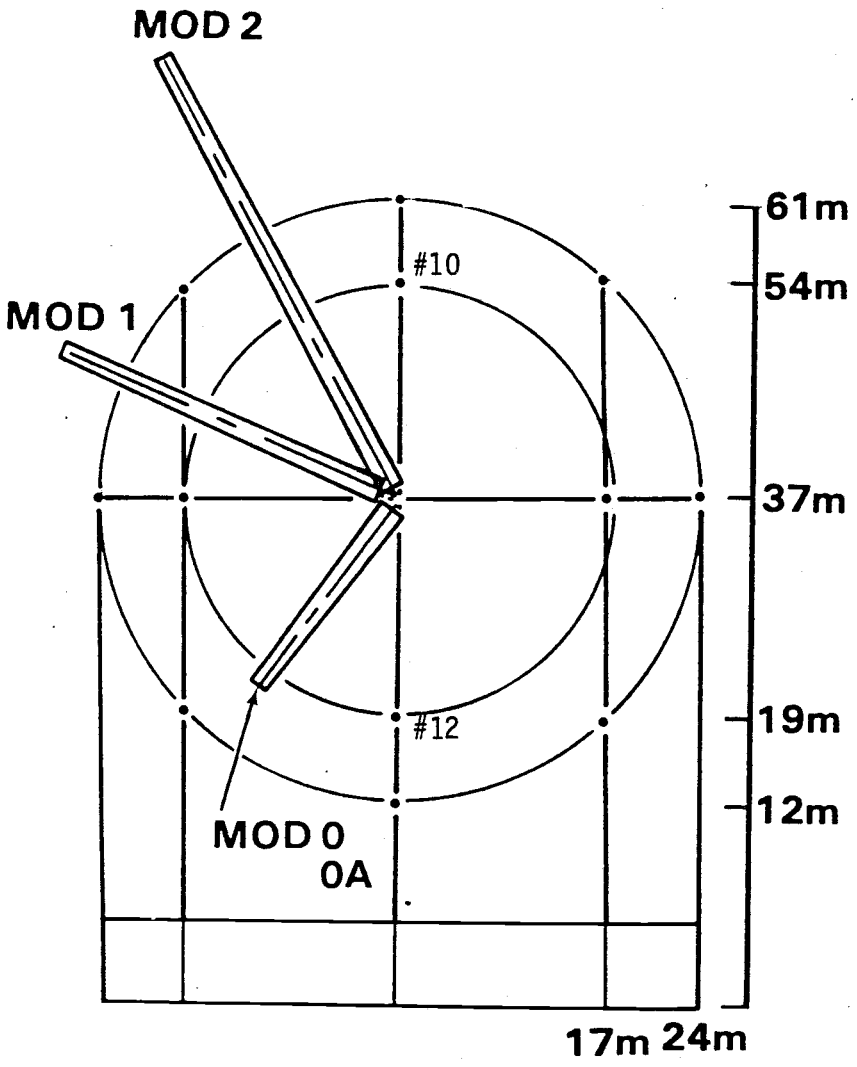

Figure 4.11. Scale Drawing of the 49 m Diameter Vertical Plane Array of Anemometers used at the Pacific Northwest Laboratory

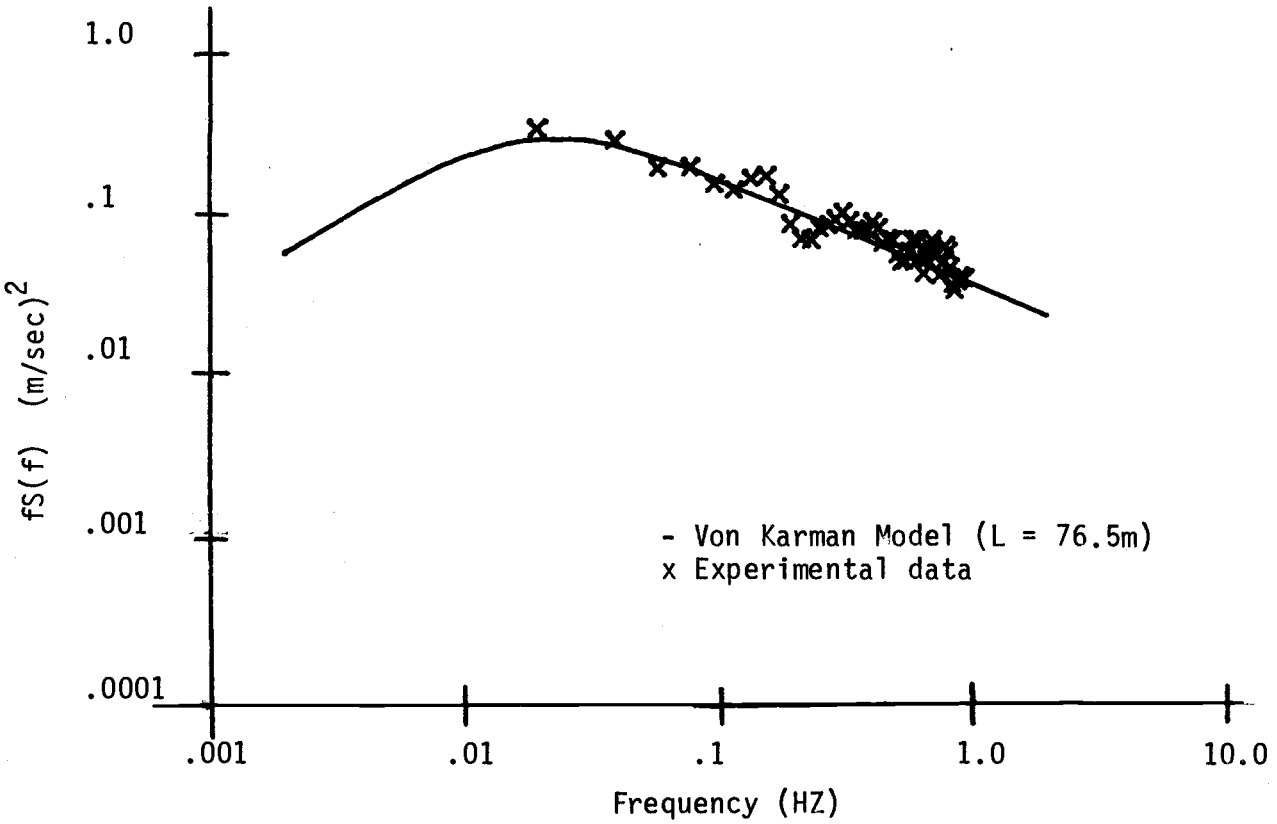

Figure 4.12. Windspeed Spectra for PNL Data

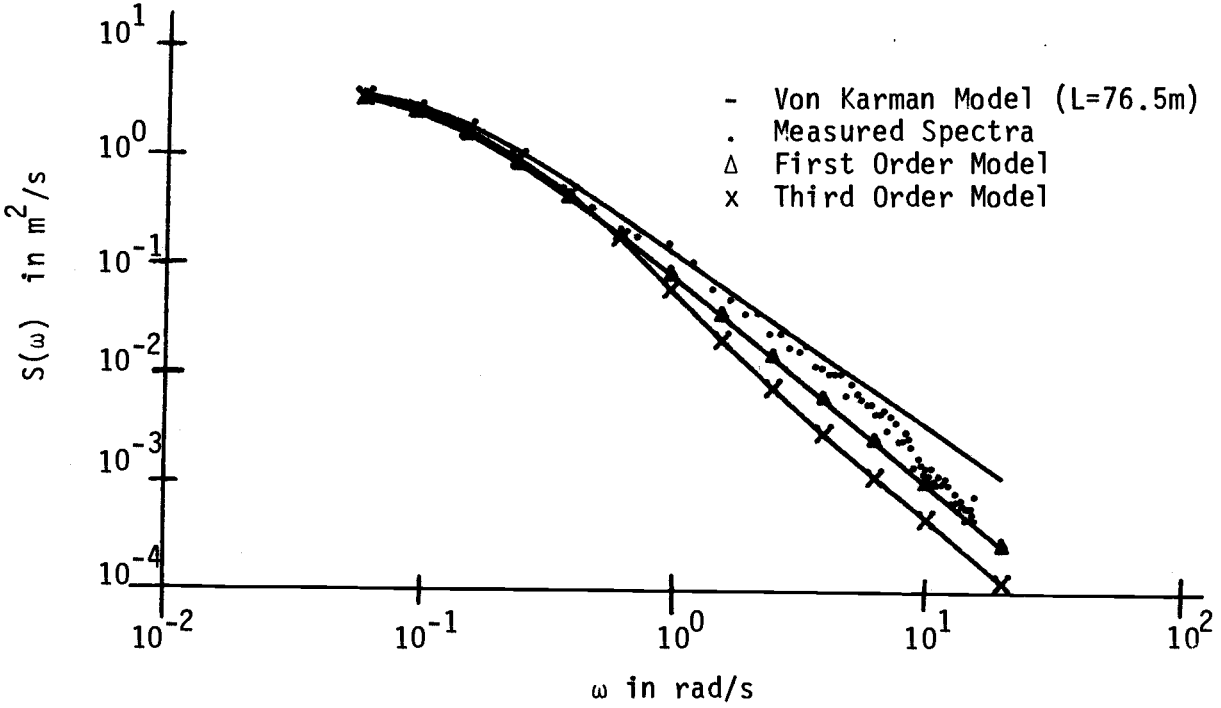

Figure 4.13. Power Spectral Density for V_y

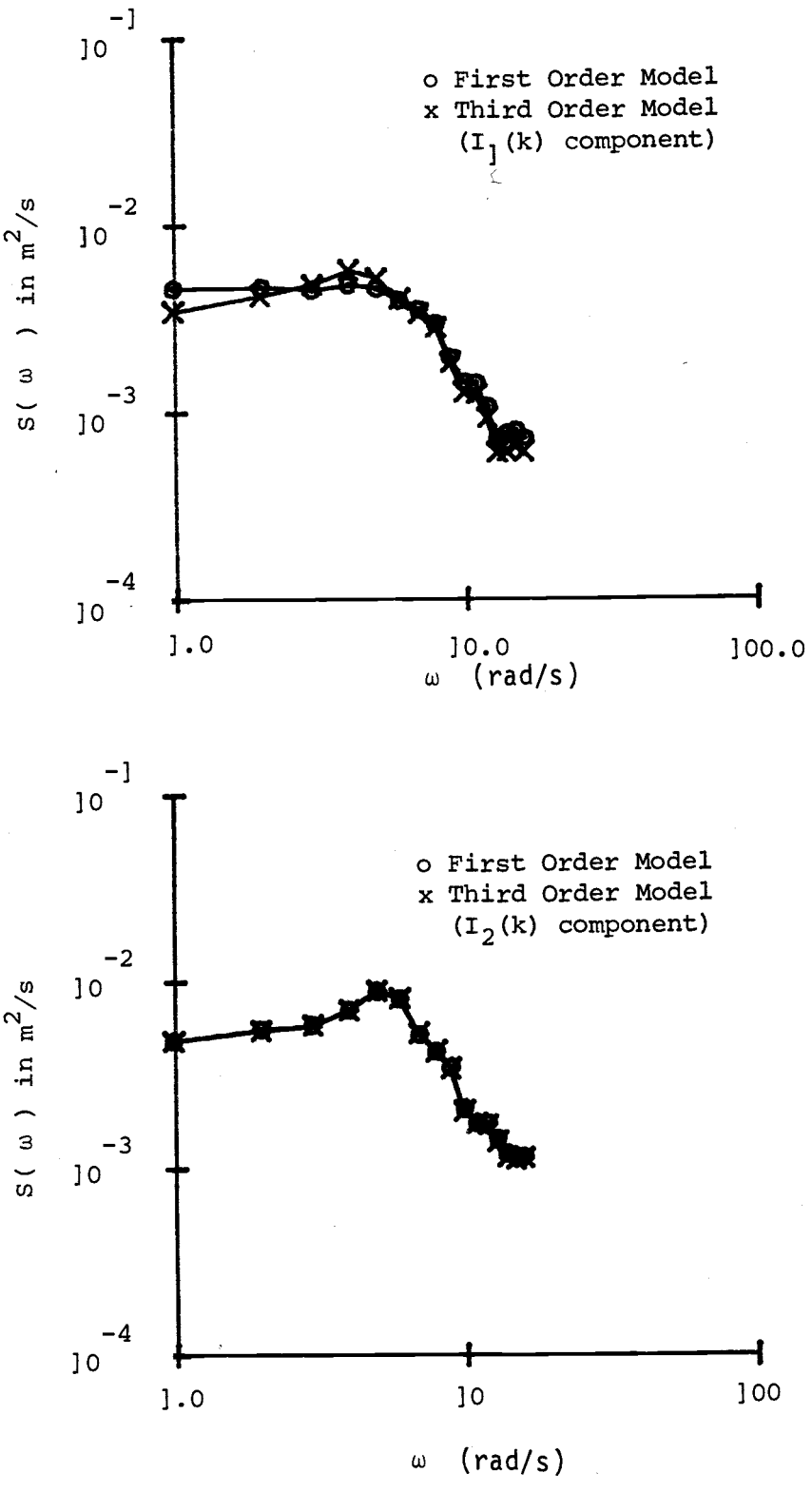

Figure 4.14. Power Spectral Density for I(k) at #10

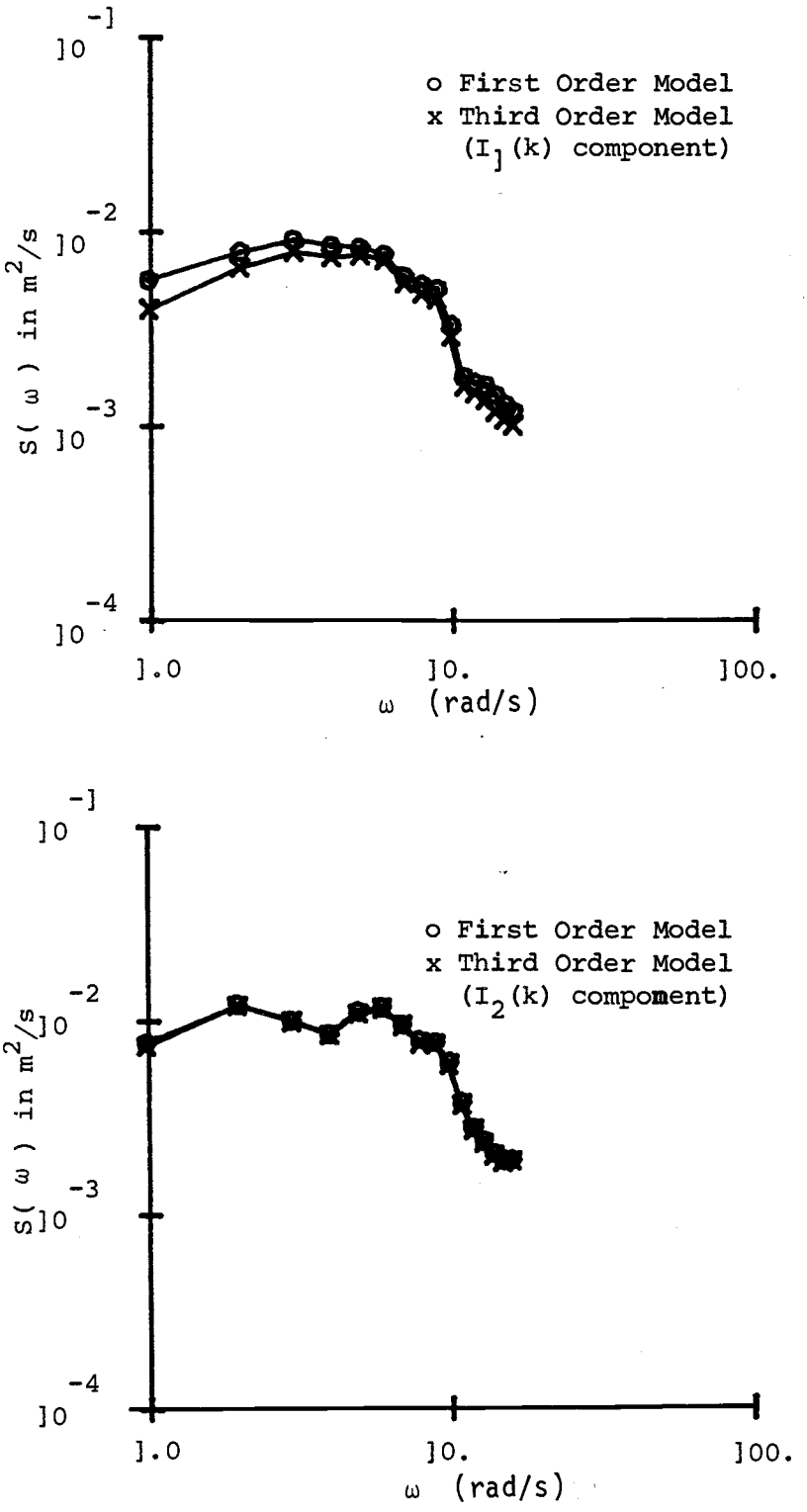

Figure 4.15. Power Spectral Density for I(k) at #12

V. CONCLUSIONS

Two approximate models for atmospheric turbulence in a wind turbine rotor disk have been presented in this research. These two models show reasonable agreement with the Von Karman model and with the experimental data. The first model is the first order uncorrelated model which assumes all twelve turbulence terms are mutually uncorrelated. The major advantage of the first order model is the relative simplicity in representing the correlation characteristics in either the time or frequency domains. The disadvantages are 1) it does not precisely satisfy the continuity equation and 2) there is no correlation between V_y and $V_{y,rr}$.

For coping with these disadvantages, the second model was proposed to satisfy the continuity equation and account for the correlation between V_y and $V_{y,rr}$. In this model V_y, $\bar{\epsilon}_{zx}$ and $V_{y,rr}$ are correlated as a third order stochastic differential equation, while the rest of the turbulence terms remain mutually uncorrelated. The third order model improves the accuracy of the turbulent $\bar{\epsilon}_{zx}$ term for the system. More parameters needed and additional computational complexity when compared to the first order model is the disadvantage to the third order model.

In the experimental data verification the results show that the third order model gives a slightly better approximation than the first order model. Even so both models are expected to give good

approximate results when they are applied to find the aerodynamic forces and moments which are caused by the turbulence. Here the first order model is recommended as the wind input model for the horizontal axis wind turbines, since it has fewer parameters than the third order model and is easy to implement to find the correlation characteristics of the wind turbulence in either time or frequency domains.

REFERENCES

1. Lumley, J. L. and Panofsky, H. A., The Structure of Atmospheric Turbulence, John Wiley & Sons, Inc. (1964), p. 4.

2. Panofsky, H. A. and Dutton, J. A., Atmospheric Turbulence, John Wiley & Sons, Inc. (1984), p. 3-4.

3. Thresher, R. W., Holley, W. E., Hershberg, E. L., and Lin, S. R., Response of the Mod-DA Wind Turbine Rotor to Turbulent Atmospheric Wind. Oregon State University, Department of Engineering and U.S. Dept. of Energy, Report DDE/RL/10378-82/1, Oct. 1983.

4. Dutton, J. A., "Effects of Turbulence on Aeronautical Systems," Progress in Aerospace Sciences, Vol. 11, Pergamon Press, Oxford, 1970, pp. 67-109.

5. Lumley and Panofsky (1964), op. cit., p. 56.

6. Holley, W. E. and Bryson, A. E., Wind Modeling and Lateral Aircraft Control for Automatic Landing, Dept. of Aero and Astro, Stanford University, SUDAAR #489 (1975), p. 3.

7. Taylor, G. I., "The Spectrum of Turbulence," Proc. Roy. Soc., Vol. A164 (1938), p. 476.

8. Holley and Bryson (1975), op. cit., p. 3-7.

9. Dutton (1970), op. cit., p. 72-73.

10. Counihan, J., "Adiabatic Atmospheric Boundary Layers: A Review and Analysis of Data from The Period 1880-1972," Atmospheric Environment, Vol. 9 (1975), p.884.

11. Panofsky, H. A. and Dutton, J. A., Atmospheric Turbulence: Models and Methods for Engineering Applications, John Wiley & Sons, Inc. (1984), p. 96.

12. Kolmogorov, A. N., "The Local Structure of Turbulence in Incompressible Viscous Fluid for Very Large Reynolds Numbers," Doklady ANSSSR, Vol. 30 (1941), p. 301.

13. Lumley and Panofsky (1964), op. cit., pp. 83-84.

14. Kolmogorov (1941), op. cit.

15. Counihan (1975), op. cit., p. 880.

16. Kaimal, J. C. et al,, Spectral Characteristics of Surface Layer Turbulence," Quart. J. Roy. Met. Soc., Vol. 98 (1972), p. 565.

17. Von Karman, T., "Sur la Theorie Statistique de la Turbulence," Comptes Rendus des Seanies de l'Acadie de Scienus, Vol. 226 (1948), pp. 2108-2111.

18. Batchelor, G. K., The Theory of Homogeneous Turbulence, Cambridge Univ. Press, Cambridge (1953), pp. 169-187.

19. Etkin, B., Dynamics of Atmospheric Flight, John Wiley & Sons (1972), pp. 533-539.

20. Holley and Bryson (1975), op. cit., p. 5.

21. Davenport, A. G., "The Spectrum of Horizontal Gustiness Near the Ground in High Winds," Quart. J. Roy. Met. Soc., Vol. 87 (1961), pp. 194-211.

22. Gradshteyn, I. S. and Ryzhik, I. M., Table of Integrals Series and Products, Academic Press, 4th Ed. (1965), p. 756.

23. Dryden, H. L., "Turbulence Investigations at the National Bureau of Standards," Proc. 5th International Congress of Applied Mechanics (1938), p. 365.

24. Etkin, B., "A Theory of the Response of Airplanes to Random Atmospheric Turbulence," J. of the Aero/Space Sciences (1959), pp. 409-420.

25. Skelton, G. B., Investigation of the Effects of Gusts on V/STOL Craft in Transition and Hover, AFFDL-TR-68-85 (1968).

26. Holley and Bryson (1975), loc. cit., pp. 16-48.

27. Thresher, R. W., Holley, W. E., Smith, C. E., Jafarey, N., and Lin, S. R., Modeling the Response of Wind Turbines to Atmospheric Turbulence, Oregon State University, Dept. of Mechanical Engineering, Report RLO/2227-81/2, Aug. 1981, Chapter 4.

28. Papoulis, A., Probability, Random Variables, and Stochastic Processes, McGraw-Hill (1965), pp. 260-263.

29. Thresher, R. W. and Holley, W. E., The Response Sensitivity of Wind Turbines to Atmospheric Turbulence, Oregon State University, Dept. of Mechanical Engineering, Report RLO/2227-81/1, May, 1981.

30. Thresher, R. W. et al., (1981), p. 71.

31. Fichtl, G. H., Covariance Statistics of Turbulence Velocity Components for Wind Energy Conversion System Design--Homogeneous, Isotropic Case, Battelle, Pacific Northwest Laboratory, PNL-3499, 1983, pp. 24-26.

32. Kwakernaak, H. and Sivan, R., Linear Optimal Control Systems, Wiley, 1972, p. 104.

33. Isaacson, E. and Keller, H. B., Analysis of Numerical Methods, Wiley, 1966, p. 54.

34. Holley, W. E., Thresher, R. W. and Lin, S. R., Atmospheric Turbulence Inputs for Horizontal Axis Wind Turbines, Proc. European Wind Energy Conf., Hamburg, Germain, Oct. 1984.

35. Papoulis, A. (1965), op. cit., pp. 516-524.

36. Chen, C. T., Introduction to Linear System Theory, 1970, Holt, Rinehart and Winston Inc., pp. 43-44.

37. Connell, J. R., The Spectrum of Wind Speed Fluctuations Encountered by a Rotating Blade of a Wind Energy Conversion System: Observations and Theory, Pacific Northwest Laboratory, November 1981, pp. 1-3.

38. Holley, W. E. and Thresher, R. W., Atmospheric Turbulence Parameters for Modeling Wind Turbine Dynamics, Proc. Large Horizontal-Axis Wind Turbine Workshop, NASA/DOE, Cleveland, Ohio, July 28-30, 1981.

39. Chen, C. T. (1970), op. cit. p. 131.

40. Kaminski, P. G., Square Root Filtering and Smoothing for Discrete Processes, Ph.D. dissertation, Dept. Aero., Astro., Stanford Univ., Stanford, Calif., Sep. 1971.

41. Kalman, R. E., "A New Approach to Linear Filtering and Prediction Problem," Trans ASME, Vol. 82D, 1960, pp. 35-50.

42. Fraser, D. C., "A New Technique for the Optimal Smoothing of Data," MIT Instrumentation Lab. T-474, Cambridge, Mass., Jan. 1967, p. 114.

43. Battin, R. H., Astronautical Guidance, McGraw-Hill, New York, 1964, pp. 338-339.

44. Kaminski, P. G., A. E. Bryson, and S. F. Schmidt, "Discrete Square Root Filtering: A Survey of Current Techniques," IEEE Trans. Automatic Control, Vol. AC-16, No. 6, Dec. 1971, pp. 727-735.

45. Bierman, G. J., "A Comparison of Discrete Linear Filtering Algorithms," IEEE Trans Aerospace and Electronic Systems, Vol. AES-9, No. 1, Jan. 1973, pp. 28-37.

46. Kaminski, P. G. (1971), loc. cit., pp. 41-42.

47. Cox, H. C., "On the Estimation of State Variables and Parameters for Noisy Dynámic Systems," IEEEE Trans. Automatic Control, Vol. AC-9, Jan. 1964, pp. 5-12.

48. Meditch, J., Stochastic Optimal Linear Estimation and Control, McGraw-Hill, New York, 1969.

49. Kaminski, P. G. (1971), loc. cit., pp. 103-104.

APPENDICES

APPENDIX A. NUMERICAL PROCEDURES USED IN THE DEVELOPMENT OF THE TURBULENCE MODEL

A.1 Area Integration over Rotor Disk

Two Gaussian quadrature formulas (1) were utilized to perform area integrations over the rotor disk. These formulas have the following form:

$$\int_A f(r,\theta)dA \approx \sum_{i=1}^{n} \sum_{j=1}^{4n} C_i f(r_i,\theta_j) \qquad (A.1)$$

where $\theta_j = \frac{\pi j}{2n}$.

The values of r_i and C_i are given in Tables A.1 and A.2, where the values of r_i are expressed as fractions of the disk radius. The distribution of points is shown in Figure A.1.

A six-point formula was also developed to reduce the computational load. For this formula, the radial location of the six points are adjusted until the best match between computations using the 64-point formula and the six-point formula was achieved. This procedure resulted in $r_i = 0.69$, expressed as a fraction of the disk radius. The distribution of the six points is also shown in Figure A.1.

For all computations using the disk area integrations, a comparison was made between two formulas to verify accuracy to within five percent.

Table A.1. Sixteen-Point Formula

r_i	C_i
.45970085	.19634954
.88807383	.19634954

Table A.2. Sixty-four-Point Formula

r_i	C_i
.26349923	.03415057
.57446451	.06402420
.81852949	.06402420
.96465961	.03415057

A.2 Radial Integrations

An eight-point Gaussian quadrature formula (2) was utilized for radial integrations.

$$\int_0^1 f(r)dr = \sum_{i=1}^{8} C_i f(r_i) \qquad \text{(A.2)}$$

The weights and absissas are given in Table A.3.

Table A.3. Radial Quadrature Formula

r_i	C_i
.0198550717	.0506142681
.1016667612	.1111905172
.2372337950	.1568533229
.4082826787	.1813418916
.5917173212	.1813418916
.7627662049	.1568533229
.8983332387	.1111905172
.9801449281	.0506142681

A.3 Fourier Transforms

For the calculation of power spectral densities from the autocorrelation function the Fourier transform defined by

$$S(\omega) = \int_{-\infty}^{+\infty} e^{-i\omega\tau} R(\tau)d\tau \qquad (A.3)$$

was numerically computed from the autocorrelation function using the finite approximation

$$S(\omega_k) = \frac{T}{2n}\left(2\mathrm{Re}\left[\sum_{j=0}^{n} R(T_j)e^{-i\omega_k\tau_j}\right]-R(o)\right) \qquad (A.4)$$

where $\omega_k = \left(\frac{4\pi n}{T(n+1)}\right)k$

$\tau_j = \left(\frac{T}{2n}\right)j$

The fast Fourier transform techniques of the IMSL (3) library routine FFTRC were utilized. Several different time intervals, T, were chosen to give overlapping spectra over the different frequency decades.

A.4 Spectra at Zero Frequency

To calculate the zero frequency power spectra, a Gaussian quadrature formula (4) was utilized for the required semiinfinite time integral.

$$\int_0^\infty e^{-x} f(x)dx = \sum_{i=1}^{n} C_i f(x_i) \qquad (A.5)$$

The absissas and weights for the 16 points are given in Table A.4.

Table A.4. Semi-Infinite Interval Quadrature Formula

x_i	C_i
0.087649	0.206152
0.46270	0.331058
1.14106	0.265796
2.12928	0.136297
3.43709	0.473289 E-01
5.07802	0.113000 E-01
7.07034	0.184910 E-02
9.43831	0.204272 E-03
12.21422	0.148446 E-04
15.44153	0.682832 E-06
19.18016	0.188100 E-07
23.51591	0.286235 E-09
28.57873	0.212708 E-11
34.58340	0.629797 E-14
41.94045	0.505047 E-17
51.70116	0.416146 E-21

A.5 Von Karman Correlation Function

Central to all of the previous numerical integration procedures is the need to compute the integrand. In this case the integrand will involve the evaluation of

$$f(\mu) = b(\frac{\mu}{a})^{1/3} K_{1/3}(\frac{\mu}{a}) \tag{A.6}$$

and

$$g(\mu) = \frac{1}{2}\mu\frac{df}{d\mu} \tag{A.7}$$

where $k_{1/3}(\cdot)$ = Modified Bessel function order of 1/3. These functions are evaluated by the subroutine VK developed by Holley and Bryson (5). The method utilizes spline interpolation and asymptotic expansion giving a result accurate to six singificant figures over a wide range of arguments.

A.6 References

1. Pierce, W. H., "Numerical Integration over the Planar Annulus," J. Soc. Indust. Appl. Math., V. 5 (1957), pp. 66-73.

2. Stroud, A. H. and Secrest, D., Gaussian Quadrature Formulas, Prentice-Hall (1966), p. 256.

3. The IMSL Library, 1979; IMSL, Inc., Sixth Floor, GNB Bldg., 7500 bellaire Blvd., Houston, TX 77036.

4. Stroud (1966) loc. cit.

5. Holley, W. E. and Bryson, A. E., Wind Modeling and Lateral Aircraft Control for Automatic Landing, Dept. of Aeronautics and Astronautics, Stanford Univ. SUDAAR No. 489 (1975), pp. 75-80.

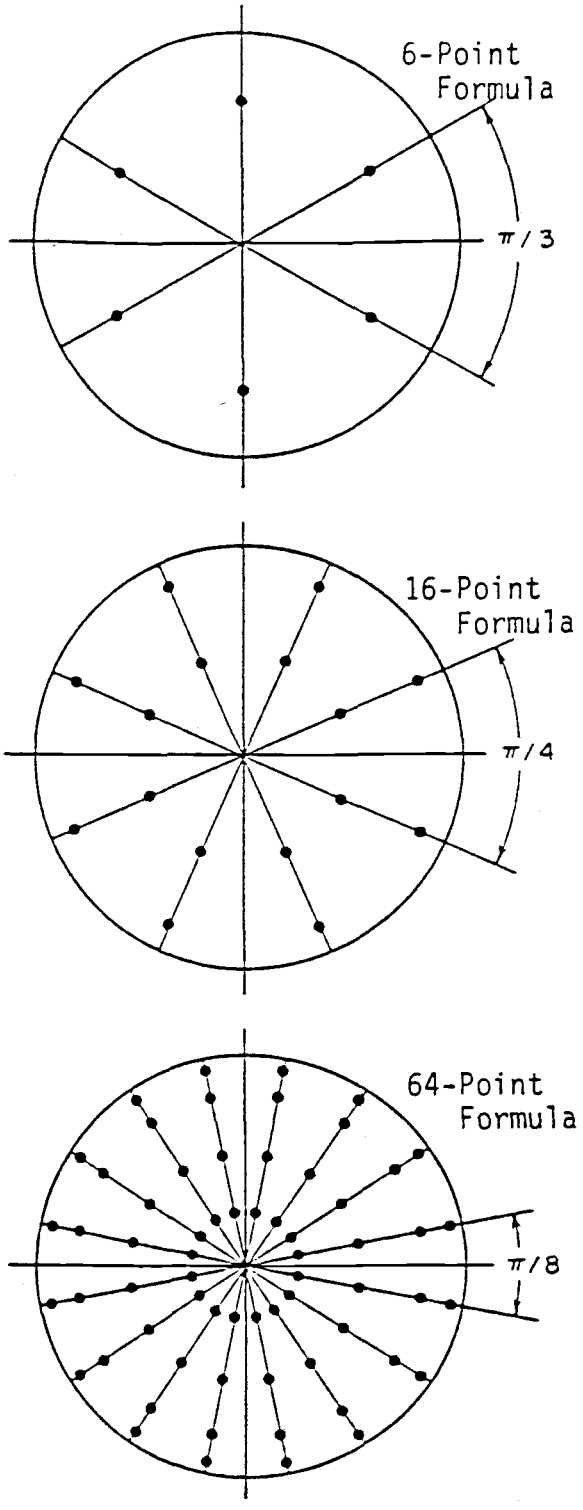

Figure A.1. Point Distribution for Disk Area Integrations

APPENDIX B. UPPER TRIANGULAR CHOLESKY FACTORIZATION

If P is a symmetric, positive definite nxn matrix, then $P = UU^T$, with U upper triangular matrix. Using the correspondence with the scaler case, U is often called the square root, or Cholesky square root of P. The factorization (1) with positive diagonal elements is given by:

For j = n, n-1, ..., 2, recursively cycle through the following equations:

$$U(j,j) = P(j,j)^{1/2}$$

$$U(k,j) = P(k,j)/U(j,j), \qquad k = 1, \ldots, j-1$$

$$P(i,k) = P(i,k) - U(i,j)U(k,j), \qquad k = 1, \ldots, j-1; \quad i = 1, \ldots, k$$

and then set

$$U(1,1) = P(1,1)^{1/2}$$

B.1 Reference

1. Bierman, G. J., Factorization Methods for Discrete Sequential Estimation, Academic Press, 1977, p. 51.

APPENDIX C. LINEAR LEAST-SQUARES REGRESSION (1)

For the general regression problem, the form of the relation

$$y = f(x,a) \tag{C.1}$$

where: x = independent variable

a = vector of parameters

y = dependent variable

is known and it is desired to determine the vector of parameters, a, when several data points (x_i,y_i) are given. In the case where the parameters appear linearly, i.e.,

$$y = a_1 f_1(x) + a_2 f_2(x) + \ldots + a_n f_n(x) \tag{C.2}$$

the data and parameters form a set of linear equations given by

$$\sum_{j=1}^{n} f_j(x_i) a_j = y_i \qquad i = 1, \ldots, m \tag{C.3}$$

When there are more data points than unknown parameters (i.e., $m > n$) the equations are overdetermined and it is unlikely that all equations can be satisfied exactly. When $m < n$ the equations are underdetermined and many different sets of parameter values can be found which fit the data exactly. To determine a reasonable solution to the problem, the parameters can be chosen to minimize the sum of the squares of the residuals, i.e.,

$$\text{Min}_a \sum_{i=1}^{m} (y_i - f(x_i,a))^2 \tag{C.4}$$

It can be shown (2), in the case when the data are given exacly by

$$y_i = F(x,a_*) + e_i \qquad (C.5)$$

where a_* are the true parameters and e_i are mutually independent random errors which are normally distributed with zero mean, that the least-squares solution is equivalent to choosing the most probable values of a, given the data (assuming no prior knowledge of a). In cases when there are more parameters than data (i.e., $m < n$) it is reasonable to set the last n-m parameters to zero then to determine the remaining m parameters which fit the data exactly.

In order to find the least squares solution, it is convenient to put the problem in matrix form

$$y - Fa = e \qquad (C.6)$$

where

$$F = \begin{bmatrix} f_1(x_1) & f_2(x_1) & \cdots \\ f_1(x_2) & \cdot & \\ \cdot & & \cdot \\ \cdot & & \cdot \\ \cdot & & \cdot \end{bmatrix}_{mxn}$$

$$y = \begin{Bmatrix} y_1 \\ \cdot \\ \cdot \\ \cdot \\ y_m \end{Bmatrix}$$

e = residual vector (dimension m)

The necessary conditions for the minimum are easily found by differentiating to be

$$2\left(\frac{\partial e}{\partial a}\right)^{T} e = 0 \tag{C.7}$$

or using Eq. (C.6) and the definition of F

$$2(-F)^{T}(y-Fa) = 0$$

or, finally

$$(F^{T}F)a = F^{T}y \tag{C.8}$$

The solution is unique when the matrix $F^{T}F$ is nonsingular.

Instead of solving Eq. (C.8) directly for

$$a = (F^{T}F)^{-1} F^{T}y \tag{C.9}$$

Golub (3) suggested using the HOuseholder (4) decomposition of the matrix F, i.e.,

$$F = QR \tag{C.10}$$

where Q is orthogonal and R has all elements below the diagonal equal to zero. Thus, Eq. (C.8) can be rewritten as

$$(QR)^{T}(QR)a = (QR)^{T}y \tag{C.11}$$

or since Q is orthogonal (i.e., $Q^{-1} = Q^{T}$)

$$(R^{T}R)a = R^{T}Q^{T}y \tag{C.12}$$

For the case when $m > n$, R is of the form

$$R = \begin{bmatrix} U \\ \cdots \\ O \end{bmatrix}$$

where U is upper triangular, and the coefficient matrix for a becomes

$$R^T R = U^T U \tag{C.13}$$

Now, let the right hand side be partitioned so that

$$Q^T y = \begin{Bmatrix} z_1 \\ \cdots \\ z_2 \end{Bmatrix} \tag{C.14}$$

Since U and F have the same rank = n, Eq. (C.14) becomes

$$Ua = z_1 \tag{C.15}$$

The solution to Eq. (C.15) involves only a simple back substitution since U is triangular.

This procedure has been implemented in a standard library subroutine supplied by the IMSL (5) and is utilized to compute a cubic polynomial approximation to the wind turbine blade section data for use in the integrations required for the aerodynamic coefficients in the wind turbine model. An equivalent procedure was utilized to compute the regression parameters in the turbulence model.

C.1 References

1. Lawson, C. L. and Hanson, R. J., Solving Least Squares Problems, Prentice-Hall, 1974.

2. Goodwin, G. C. and Payne, R. L., Dynamic System Identification, Academic Press, 1977, pp. 29-41.

3. Golub, G., "Numerical Method for Solving Linear Least Squares Problems," Numerische Mathematik, V. 7, 1965, pp. 206-216.

4. Householder, A. S., "Unitary Triangularization of a Nonsymmetric Matrix," J. Assn. Comput. Mach., V. 5, 1958, pp. 339-342.

5. Anon., Documentation for Routine LLSQF, The International Mathematical and Statistical Library, IMSL, Inc., Houston, TX.

APPENDIX D. POWER SPECTRA ESTIMATES FROM DATA VIA FFT COMPUTATIONS

D.1 Spectral Density via Finite Fourier Transforms

Consider a pair of associated sample records $x_k(t)$ and $y_k(t)$ from stationary random processes $\{x_k(t)\}$ and $\{y_k(t)\}$. For a finite time interval $0 \leq t \leq T$, define

$$S_{xy}(f,T,k) = \frac{1}{T} X_k^*(f,T) Y_k(f,T) \tag{D.1}$$

where

$$X_k(f,T) = \int_0^T x_k(t) e^{-j2\pi ft}\, dt$$

$$Y_k(f,T) = \int_0^T y_k(t) e^{-j2\pi ft}\, dt$$

The quantities $X_k(f,T)$ and $Y_k(f,T)$ represent finite Fourier transforms of $x_k(t)$ and $y_k(t)$ respectively, and $X_k^*(f,T)$ is the complex conjugate of $X_k(f,T)$.

The two sided cross-spectral density function is given by the limit (1,2)

$$S_{xy}(f) = \lim_{T\to\infty} E[S_{xy}(f,T,k)] \tag{D.2}$$

where $E[S_{xy}(f,T,k)]$ is the expected value operation over the ensemble index k.

In case of x=y, the power spectral density function is

$$S_x(f) = \lim_{T\to\infty} \frac{1}{T} E[|X_k(f,T)|^2] \qquad (D.3)$$

The finite-range Fourier transform will exist as defined by

$$X(f,T) = \int_0^T x(k)e^{-j2\pi ft}\,dt \qquad (D.4)$$

Assume now that x(t) is sampled at N equally spaced points a distance h apart. The discrete version of Eq. (D.4) is

$$X(f,T) = h \sum_{N=0}^{N-1} x_n \exp[-j2\pi fnh] \qquad (D.5)$$

where $x_n = x(nh)$ $n = 0,1,2, \ldots, N-1$

The usual selection of discrete frequency values for the computation of X(f,T) is

$$f_k = kf = \frac{k}{R} = \frac{k}{Nh}, \qquad k = 0,1, \ldots, N-1 \qquad (D.6)$$

At these frequencies, the transformed values give the Fourier components defined by

$$X_k = \frac{X(f_k,T)}{h} = \sum_{n=0}^{N-1} x_n \exp\left[-j\frac{2\pi kn}{N}\right], \quad k = 0,1, \ldots, N-1 \qquad (D.7)$$

Note that results are unique only out to k = N/2 since the Nyquist cutoff frequency occurs at this point. Fast Fourier transform (FFT) methods are designed to compute these quantities, X_k.

D.2 Power Spectra Estimates

For a single record x(t), a raw estimate of the power spectral density function at any frequency f is given by

$$\tilde{S}_x = \frac{1}{T} E[|X(f,T)|^2] \tag{D.8}$$

Here, T = nh and from Eq. (D.7)

$$X(f,T) = h \sum_{n=0}^{N-1} x_n \exp[-j2\pi fnh] \tag{D.9}$$

At the usual FFT discrete frequency values (Eq. D.6) the Fourier components are defined in Eq. (D.7). Hence, from Eqs. (D.8) and (D.7), the power spectrum estimate becomes

$$\begin{aligned} \tilde{S}_x &= \frac{1}{Nh}|X(f_k,T)|^2 \\ &= \frac{h}{N}|X_k|^2 \end{aligned} \tag{D.10}$$

D.3 Procedural Steps (3,4)

The following steps are recommended to compute power spectra estimates via FFT procedures. Assume that the sample size for the data sequence x_n is initially of arbitrary size N.

1. Truncate the data sequence or add zeros so that $N = 2^p$.
2. Taper the resulting sequence using the cosine taper data window or some other appropriate tapering.
3. Compute the X_k of Eq. (D.7) for k = 0,1, ..., N-1, using the FFT method.
4. Compute $\tilde{S}_k$ of Eq. (D.10) for k = 0,1, ..., N-1.
5. Adjust these estimates for the scale factor due to tapering, e.g., by replacing $\tilde{G}_k$ by (1/0.875) $\tilde{G}_k$ if the cosine taper data window is used.

These adjusted estimates are raw estimates of the power spectral density function. Frequency smoothing, segment averaging or combined averaging (5) should be implemented to obtain final practical smooth estimates which have more suitable statistical variability properties.

D.4 References

1. Bendat, J. S. and Piersol, A. G., Random Data: Analysis and Measurement Procedures, John Wiley & Sons Inc., 1971, pp. 82-85.

2. Newland, D. E., An Introduction to Random Vibrations and Spectral Analysis, Logman, 1975, p. 133.

3. Bendat and Piersol (1971), op. cit., pp. 326-327.

4. Newland (1975), op. cit., pp. 142-145.

5. Bendat and Piersol (1971), op. cit., pp. 328-329.

APPENDIX E. ALGORITHM FOR COMPUTING DISCRETE WHITE NOISE EXCITATION

Consider the state equation

$$\dot{x}(t) = Ax(t) + BW(t), \qquad x(0) = x_0 \tag{E.1}$$

where $w(t)$ is Gaussian random noise with zero mean and flat PSD = S_w.

The solution of Eq. (E.1) is given by

$$x(t) = \phi(t)\, X_0 + \int_0^t \phi(t-\tau)BW(\tau)d\tau \tag{E.2}$$

where ϕ is the state transition matrix.

Using Eq. (E.2) the sampled state satisfies the difference equation

$$x(k+1) = \phi(\Delta)x(k) + \xi(k) \tag{E.3}$$

where Δ = Sampling period

$$\xi(k) = \int_0^{\Delta} \phi(\Delta-\tau)BW(t_k+\tau)d\tau$$

The mean of the sequence $\xi(k)$ is

$$E[\xi(k)] = E\left[\int_0^{\Delta} \phi(\Delta-\tau)BW(t_k+\tau)d\tau\right]$$

$$= \int_0^{\Delta} \phi(\Delta-\tau)B\ E[W(t_k+\tau)]d\tau$$

$$= 0 \qquad \text{(Since } E[W]=0\text{)}$$

And the auto and cross correlation function are

$$E[\xi(k)\xi^T(k)] = E[(\int_0^\Delta \phi(\Delta-\tau)BW(t_k+\tau)d\tau)(\int_0^\Delta \phi(\Delta-\sigma)BW(t_k+\sigma)d\sigma)^T]$$

$$= \int_0^\Delta\int_0^\Delta \phi(\Delta-\tau)B\ E[W(t_k+\tau)W^T(t_k+\sigma)]B^T\phi^T(\Delta-\sigma)d\tau d\sigma$$

$$= \int_0^\Delta \phi(\Delta-\tau)BS_wB^T\phi^T(\Delta-\tau)d\tau$$

$$= \eta(\Delta) \qquad \text{(E.4)}$$

$$E[\xi(k)\xi^T(j)] = \int_0^\Delta\int_0^\Delta \phi(\Delta-\tau)BE[W(t_k+\tau)W^T(t_j+\sigma)B^T\phi^T(\Delta-\sigma)d\tau d\sigma$$

$$= 0 \qquad \text{(Since W(t) is uncorrelated)}$$

Thus, $\xi(k)$ is normally distributed and sequentially uncorrelated random sequence. By Cholesky decomposition, Eq. (E.3) can be decomposed to

$$\eta(\Delta) = \Gamma(\Delta)\Gamma^T(\Delta) \qquad \text{(E.5)}$$

Hence,

$$\xi(k) = \Gamma(\Delta)\ u(k) \qquad \text{(E.6)}$$

where $u(k)$ is a Gaussian and uncorrelated random sequence with unit variance.

E.1 The Algorithm for Computing (1)

Let $P = BS_wB^T$ and $t = \Delta - \tau$, Eq. (E.4) becomes

$$\eta(\Delta) = \int_0^\Delta \phi(t)\, P\, \phi^T(t)dt \tag{E.7}$$

since ϕ is the state transition matrix, the unique solution of

$$\dot{\phi}(t) = A\,\phi(t), \qquad \phi(0) = I \tag{E.8}$$

we can solve

$$\begin{aligned}\phi &= e^{At} \\ &= \sum_{k=0}^{\infty} \frac{t^k A^k}{k!}\end{aligned} \tag{E.9}$$

Substituting Eq. (E.9) into Eq. (E.7) we get

$$\eta(\Delta) = \int_0^\Delta \left(\sum_{k=0}^{\infty} \frac{t^k A^k}{k!}\right) P \left(\sum_{k=0}^{\infty} \frac{t^k A^k}{k!}\right)^T dt$$

$$= \int_0^\Delta \{P + (AP+PA^T)t + [A^2P+2APA^T+P(A^T)^2]\frac{1}{2}t^2$$

$$+ \ldots\}dt$$

$$= P\Delta + (AP+PA^T)\frac{\Delta^2}{2} + (A^2P+2APA^T+P(A^T)^2)\frac{\Delta^3}{3!}$$

$$+ \ldots \tag{E.10}$$

Define the recursive relation

$$X_{k+1} = (AX_k + X_k A^T)\frac{\Delta}{k+1} \qquad (E.11)$$

with $$X_1 = P\Delta$$

Eq. (E.10) can be expressed in terms of X_k, that is

$$\eta(\Delta) = \sum_{k=1}^{\infty} X_k \qquad (E.12)$$

E.2 Reference

1. Kuo, Ting-Tung, Computer Simulation of Linear Stochastic Systems, Oregon State University, 1983.